Winter 2016

Stabilization of Compressor Surge Using Gain-Scheduled Controller

Zaid A. Alsayouri
University of New Hampshire, Durham

STABILIZATION OF COMPRESSOR SURGE USING GAIN-SCHEDULED CONTROLLER

BY

ZAID A ALSAYOURI

Bachelor of Science in Electrical Engineering, University of Jordan, 2014

THESIS

Submitted to the University of New Hampshire

in Partial Fulfillment of

the Requirement for the Degree of

Master of Science

in

Electrical Engineering

December, 2016

This thesis has been examined and approved in partial fulfillment of the requirements for the degree of Master of Science in Electrical Engineering by:

Thesis Director, Se Young Yoon, Assistant Professor

Micheal J. Carter, Associate Professor

Qiaoyan Yu, Assistant Professor

On September 2, 2016

Original approval signatures are on file with the University of New Hampshire Graduate School.

DEDICATION

I would like to dedicate my thesis to my beloved family and my friend Ahmad Kanan (RIP)

ACKNOWLEDGEMENTS

I would like to thank my advisor Dr. Se Young (Pablo) Yoon for monitoring me throughout my graduate studies, offering valuable advice, encouragement, and being a great person to work with.

Thanks also to my committee members Dr. Michael J. Carter and Dr. Qiaoyan Yu for reading my thesis and offering their comments and criticism.

Table of Contents

LIST OF TABLES

LIST OF FIGURES

ABSTRACT

STABILIZATION OF COMPRESSOR SURGE USING GAIN-SCHEDULED CONTROLLER

by

Zaid A Alsayouri

University of New Hampshire, December, 2016

Gain scheduling is a control method that is used in nonlinear systems to optimize their controlled performance and robustness over a wide range of operating conditions. It is one of the most commonly used controller design approaches for nonlinear systems. In this control technique, the controller consists of a collection of linear controllers, each of which provides satisfactory closed-loop stability and performance for a small operating region, and combined they guarantee the stability of the system along the entire operating range. The operating region of the system is determined by a scheduling signal, also known as the scheduling variable, which may be either exogenous or endogenous with respect to the plan. A good design of the gain-scheduled controller requires a suitable selection of the scheduling variables to properly reflect the dynamics of the system.

In this thesis, we apply the gain scheduling control method to the control of compression systems with active magnetic bearings (AMBs). First, a gain-scheduled controller is designed and tested for the rotor levitation control of the AMB system. The levitation controller is designed to guarantee robust rotor levitation over a wide range of rotating speeds. We show through numerical simulation that the rotor vibration is contained in the presence of uncertainties introduced by speed dependent gyroscopic forces. Next, we implement the gain scheduling control method to the active

stabilization of compressor surge in a compression system using the AMBs as actuators. Recently, Yoon et al. [1] showed that AMBs can be used to stabilize the surge instability in a compression system. In this thesis, we demonstrate that gain scheduling control can effectively extend the stable operating region of the compression system beyond the limits presented in [1]. For the stabilization of surge, a gain-scheduled controller was obtained by combining six linear controllers that together they cover the full operating range of the compression system. We were able to demonstrate through numerical simulation that the designed surge controller is effective in suppressing the instability down to a throttle valve opening of 12%, and in the presence of random flow disturbance and actuator saturation. An observer-based technique was implemented to achieve a bumpless and smooth transfer when switching between the linear controllers.

Chapter 1

Motivation

Over the last six decades, linear control methods have seen important advancements, both in terms of theory and applications. Many applications in the real world behave in a nonlinear manner, and their dynamics are approximated by linear models in order to apply linear controller design methods. On the other hand, there are some nonlinear systems, such as high performance aircraft that operates over a wide range of Mach numbers and altitudes and the wide operating range limits the accuracy of any single linearized model approximation. A common method that is used for the control of this class of nonlinear systems is to base the design on different operating conditions along the system parameter range. This is the basic idea of the gain scheduling method.

Compression systems are used in applications that require fluid or gas at high pressure. These compressors may suffer from instabilities such as rotating stall and compressor surge, which may cause significant damage to the compression system if they are not controlled properly. Recently, active magnetic bearings (AMBs) have been used along with active controllers to control these instabilities [1]. Active magnetic bearings are contactless bearings that suspend the rotor using magnetic forces. The contactless feature of the AMBs give them advantages in applications that require continuous maintenance-free operation for extended periods of time.

In this thesis, we apply the gain scheduling control method to the control of compression systems with active magnetic bearings (AMBs). First, a gain-scheduled controller is designed and

tested for the rotor levitation control of the AMB system. The levitation controller is designed to guarantee robust rotor levitation over a wide range of rotating speeds. We show through numerical simulation that the rotor vibration is contained in the presence of uncertainties introduced by speed dependent gyroscopic forces. Next, we implement the gain scheduling control method to the active stabilization of compressor surge in a compression system using the AMBs as actuators. Recently, Yoon et al. [1] showed that AMBs can be used to stabilize the surge instability in a compression system. In this thesis, we demonstrate that gain scheduling control can effectively extend the stable operating region of the compression system beyond the limits presented in [1]. For the stabilization of surge, a gain-scheduled controller was obtained by combining six linear controllers that together cover the full operating range of the compression system. We were able to demonstrate through numerical simulation that the designed surge controller is effective in suppressing the instability down to a throttle valve opening of 12%, and in the presence of random flow disturbance and actuator saturation. An observer-based technique was implemented to achieve a bumpless and smooth transfer when switching between the linear controllers.

The remainder of the thesis is organized as follows. In Chapter 2, we introduce the compression system and the most common instabilities from which compressors suffer. After that, an introduction to linear control theory is presented in Chapter 3, and $H\infty$ and μ-synthesis control methods are briefly discussed. In addition, we present an overview of the gain scheduling control, and discuss the main advantages and disadvantages. A case study where we design a gain-scheduled controller for the rotor levitation of an AMB supported motor is presented in Chapter 4. Then, we extend the results in [1] by designing a gain-scheduled controller for the stabilization of compressor surge, and simulation results are shown in Chapter 5. Finally, we present our conclusions in Chapter 6.

Chapter 2

Introduction

A compression system is used to increase the pressure of a gas. Pressure rise can be attained either by increasing the temperature so that the kinetic energy of the gas molecules increase, or by forcing the gas molecules to settle into a small volume. Compressors are driven by different power sources such as electric motors, steam turbines, gas turbines, or diesel engines. They are widely used in the industrial field and they have many applications. In this chapter, compressor types and common instabilities will be introduced. In addition, we will talk briefly about active magnetic bearings, how they work, and their application to compression systems.

2.1 Introduction to Compression Systems

Based on how the pressure rise is achieved in compressors, they can be divided into two main types: positive displacement compressors (intermittent flow) and dynamic compressors (continuous flow). On one hand, the pressure rise is achieved in positive displacement compressors by reducing the gas volume and discharging the compressed gas out of the enclosure. The most common positive displacement compressors are reciprocating compressors and rotary compressors. On the other hand, dynamic compressors achieve the pressure rise by increasing the velocity of the gas, and then restricting the gas flow in order to decelerate it. The reduction of the velocity, or the variation on the kinetic energy, is converted into pressure rise. There are two distinct types of the dynamic compressors: centrifugal compressors and axial compressors. Figure

2.1 shows the types of compressors. In the following two subsections, we will focus on the centrifugal compressor and the axial compressor.

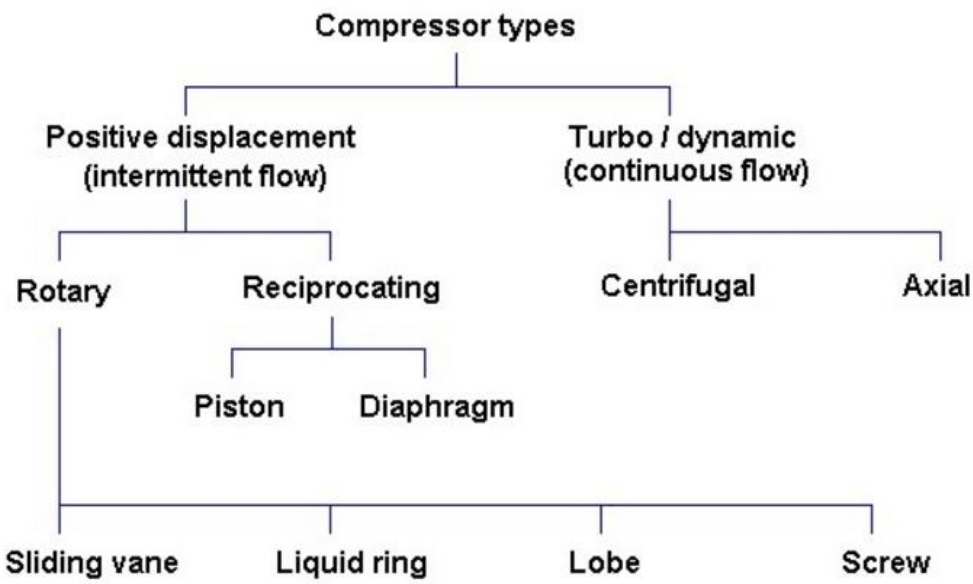

Figure 2.1 Compressors Types

2.1.1 Centrifugal Compressor

The centrifugal compressor is a dynamic compressor that is mainly used on large capacity systems [2]. It has three main components: an impeller, a diffuser, and a volute casing. Large capacity centrifugal compressors may have two or more impellers or stages in the same casing. Centrifugal compressors are usually driven by hermetic electric motors. However, open-drive centrifugal compressors are also available for some applications using steam turbine, gas turbine, or engine drives. The impeller is a circular rotating disk with curved blades that is driven to high speeds by the motor. As the gas enters the compressor, it is directed to the center of the impeller. When the impeller rotates, the gas rotates with it. This circular motion moves the gas from the center of the impeller to the impeller edge with a higher speed. As the gas leaves the outside edge

of the impeller, it enters the diffuser. The diffuser is designed so that the flow area increases as the gas leaves the impeller. This increased area allows the gas to slow down, where the kinetic energy is converted into a static pressure. Figure 2.2 illustrates a cross section of the centrifugal compressor.

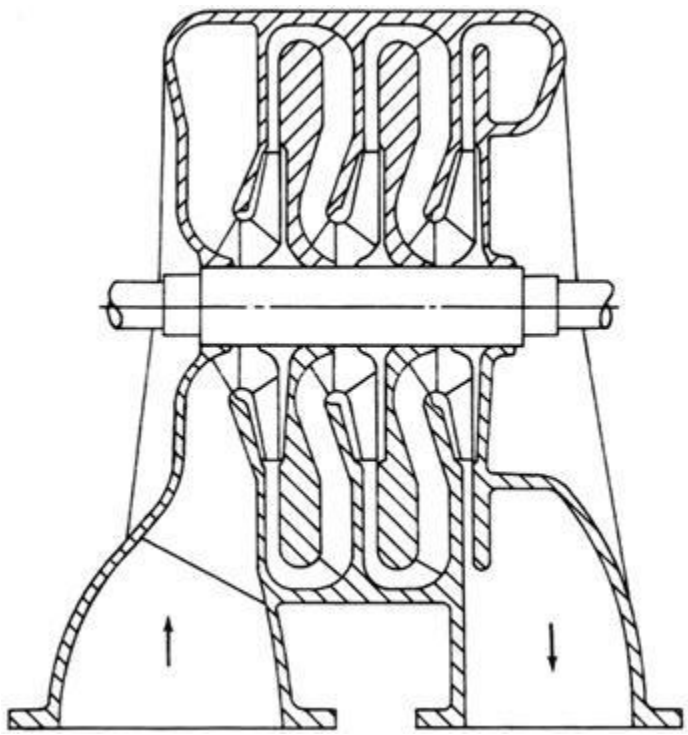

Figure 2.2 A cross section of a centrifugal compressor [31]

2.1.2 Axial Compressor

Similar to the centrifugal compressor, an axial compressor achieves gas compression by accelerating and decelerating the gas, and then transforms the kinetic energy into static pressure [3]. Axial compressors consist of a rotor and a stator. The rotor has blades that are known as the rotor blades, and the stator has blades that are known as stator blades. Usually, axial compressors are multi-staged. Each stage consists of a consecutive rotor blade and stator blade. The rotor blades accelerate the gas and pass it to the stator blades, where the gas is decelerated and the variation in

the kinetic energy is converted into a static pressure. Differently from centrifugal compressors, the flow in the axial compressor takes place in the axial direction. In addition, the axial compressors can handle higher flow rates compared to centrifugal compressors, and they are more efficient [31]. Figure 2.3 shows a cross section of the axial compressor.

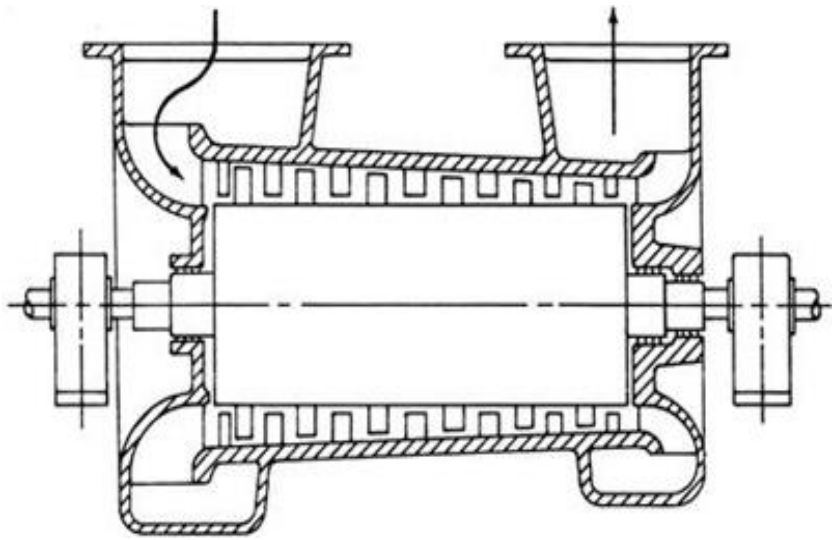

Figure 2.3 A cross section of an axial compressor [31]

2.2 Compression System Instabilities

There are two main instabilities that limit the performance and affect the efficiency and stability of compressors: rotating stall and compressor surge. In this section, we will discuss the causes and solutions for these instabilities.

2.2.1 Rotating Stall

In aircraft, stall is defined as a decrement in the lift coefficient on wings which results from the increment in the angle of attack of wings above a certain limit. This causes the aircraft to lose lift and go down. Similar to aircraft, compression systems can suffer from stall. In compression systems, the gas flow is parallel to the blades of the impeller. As the pressure becomes higher, the adverse pressure gradient on the impeller becomes higher. At a certain point, the adverse pressure

gradient on the impeller becomes very high in a way that makes the pressure separate the flow from the blades [4]. At that point, the lift force between the blades and the flow is lost and the stall occurs. This causes the back flow of the gas in the opposite direction.

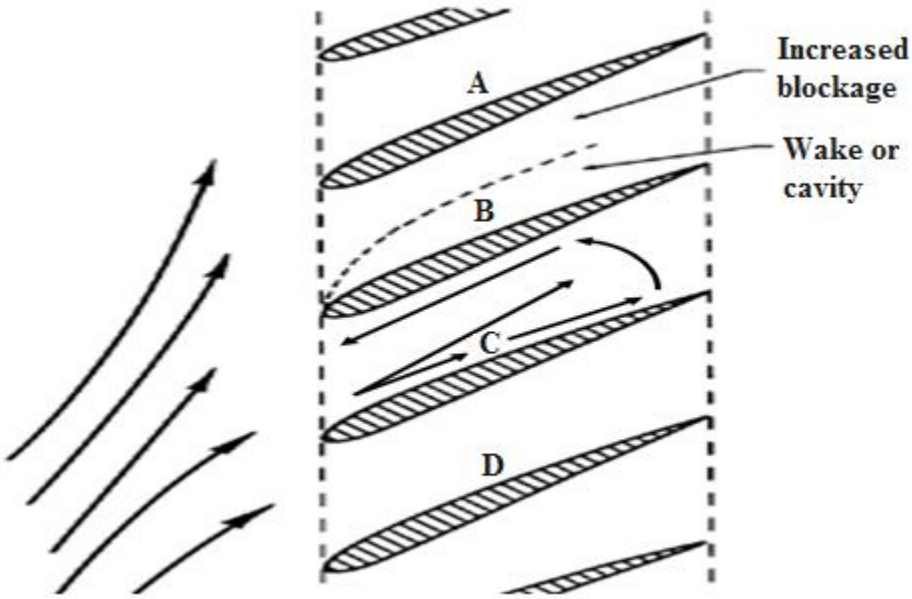

Figure 2.4 Schematic of stall cell in rotating stall [5]

Figure 2.4 illustrates a set of blades in stall condition. If blade B is stalled, a blockage of the flow will occur in the area between blades A and B. This area is called the stall cell. The blocked flow will be distributed between the other plates in the upward direction, and they will be stalled in the same manner. That is why it is called the rotating stall. The stall cells propagates in the direction of the flow. These cells rotate with the rotating blades at 50% - 70% of their speed [5].

2.2.2 Compressor Surge

Compressor surge is one of the most common dynamic instabilities that affects the performance of centrifugal and axial compressors. It occurs as a result of the continuous increment of pressure in the plenum in a way that the compressor cannot generate sufficient pressure difference to match the pressure rise in the plenum [1]. This causes the backflow of the gas towards

the compressor's inlet which initiates the surge limit cycle, and thus the system becomes unstable. The steady state gas flow and pressure condition that indicate the initiation of the surge instability in a compressor is known as the surge point. This point separates between the stable and unstable regions of the compressor characteristic curve, which maps the equilibrium operating point of the compressor in terms of pressure rise and flow rate. Figure 2.5 shows the compressor characteristic curve for different operating speeds N_1, N_2, and N_3.

There are a few symptoms which indicate that surge may be occurring in a compressor, such as low flow rate in the system, increment in the discharge gas temperature, violent fluctuation in the discharge pressure, and excessive radial vibration in the compressor. Surge might cause structural damage to compressors. Generally, there are two popular methods that are used to overcome the surge problem: surge avoidance [6] and surge control [1]. In surge avoidance, the compressor is forced to operate away from the unstable region by using a safety margin called the surge margin. If the compressor operates in the safety margin, a safety mechanism is used to release

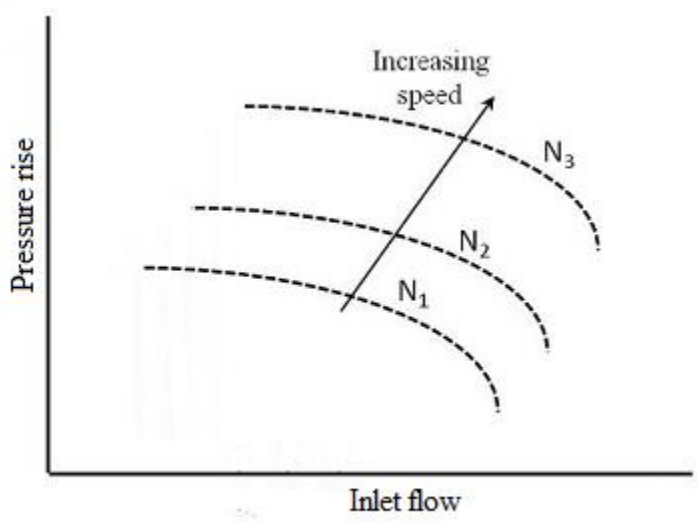

Figure 2.5 Compressor characteristic curve for different operating speeds

the built up pressure and increase the flow, which pushes the operation back towards the stable region. This method is used widely in industrial applications. The second method is surge control, in which a controller is used to regulate and stabilize the flow in the compressor when operating under surge conditions. This method will be studied in Chapter 5.

2.3 Active Magnetic Bearings in Compression Systems

An active magnetic bearing is a bearing that supports the rotating shaft using magnetic forces generated by electromagnets. This is achieved by integrating proximity sensors, controller, power amplifiers, and electromagnetic actuators [24]. The sensors measure the displacement of the rotor from its reference position, and the controller generates a control signal based on the sensor output. The control signal is then converted to a control current by the power amplifier. This control current generates a magnetic field in the actuating electromagnets, which results in magnetic forces that suspend the rotor. The main advantage of magnetic bearings is that they support the rotor without mechanical contact, and they are widely used in applications involving high speed rotating machinery. Also, the contactless feature of the AMBs allows for “canned” designs of compressors and pumps for applications involving high pressure, high temperature, and erosive chemicals. Magnetic bearings require a continuous power input and active control to keep the rotor under stable levitation [11].

2.3.1 Modeling of Flexible Rotor Dynamics

Rotors are main components in dynamic compressors that transfer energy to the working gas, and the target of the AMB actuator for levitation. For the control of the AMB levitation, an accurate model of the AMB dynamics is needed. Figure 2.6 shows a rotor that is suspended by AMB’s.

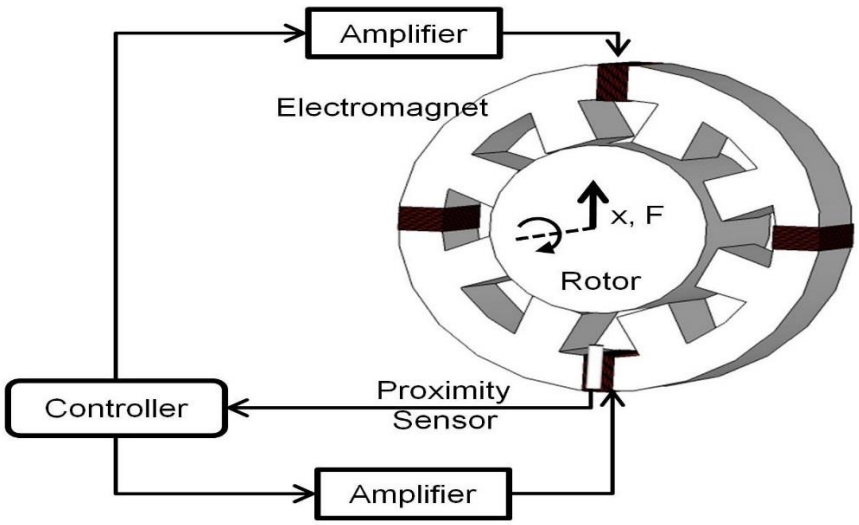

Figure 2.6 Rotor suspended by AMB's [1]

The finite element method (FEM) is used to analyze and model flexible rotors supported by AMBs. This method is used to model large scale and complex rotor systems. Using the FEM, the rotor is divided into *n* elements. Between each neighboring elements, nodes are introduced and each node has a certain number of degrees of freedom (DoF). Figure 2.7 illustrates a 2D rotor mesh example. To simplify the modelling, the following assumptions are used:

- rotor elements have a uniform radius along its length,
- the added disks are treated as point masses, and
- the rotor is symmetric in the lateral axis.

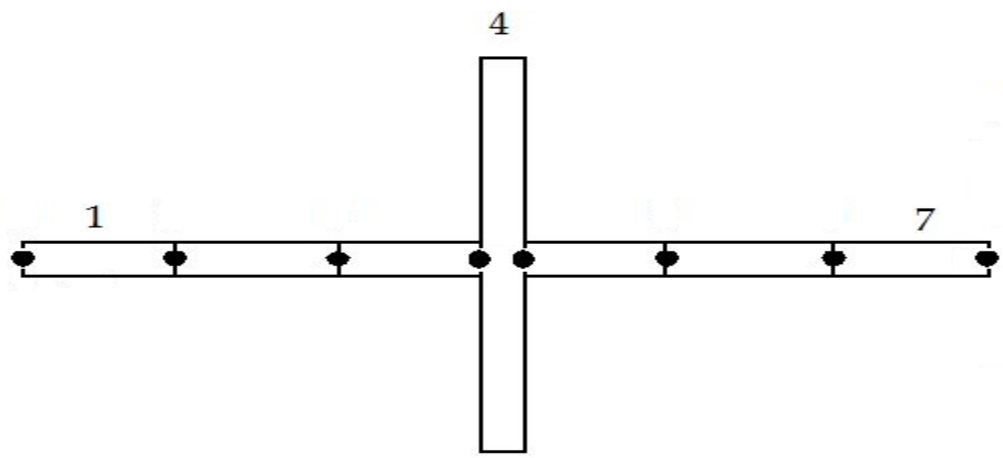

Figure 2.7 2D rotor mesh example

After the division of the shaft into smaller elements, each element is studied separately [1]. For each element, the generalized displacement and rotation are described using the DoFs at each points. For simplicity, only the lateral dynamics of the rotor will be considered, thus each element has 8 DoFs. Figure 2.8 shows a rotor element and the generalized displacement of the nodes *i* and *i*+1.

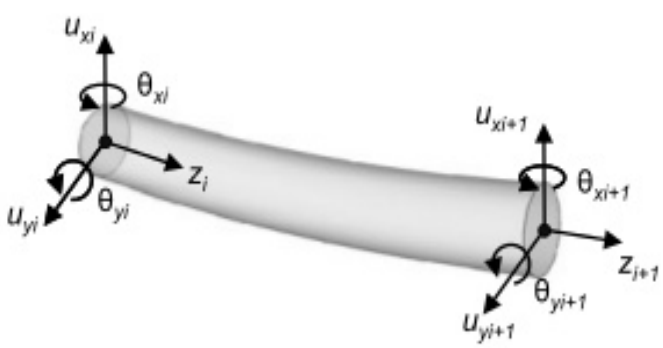

Figure 2.8 Rotor element with the generalized displacement for nodes *i* and *i*+1

As shown in Figure 2.8, the angular displacement about the x and y axes are given by Θ_x and Θ_y, respectively. In addition, the lateral displacement in the x and y axes are given by U_x and U_y, respectively. Thus the generalized displacement vector at the node *i* is given by

$$q_i = \begin{bmatrix} U_{xi} \\ U_{yi} \\ \Theta_{yi} \\ \Theta_{xi} \end{bmatrix}. \tag{2.1}$$

By combining the generalized displacement vectors at the nodes *i* and *i*+1, we get the generalized displacement vector for the *i*th element Q_i, which is defined as

$$Q_i = \begin{bmatrix} q_i \\ q_{i+1} \end{bmatrix}. \tag{2.2}$$

Based on the defined DoFs, the lateral translation and rotation along the rotor element can be interpolated, and the shape of that element is estimated using the generalized displacement vector Q_i and shape functions N_i. The shape functions are given by

$$N_1 = \frac{1}{L^3}\,(L^3 - 3z^2L + 2zL^3), \tag{2.3a}$$

$$N_2 = \frac{1}{L^2}\,(zL^2 - 2z^2L + z^3), \tag{2.3b}$$

$$N_3 = \frac{1}{L^3}\,(3z^2L - 2z^3), \tag{2.3c}$$

$$N_4 = \frac{1}{L^2}\,(-z^2L + z^3). \tag{2.3d}$$

where *L* is the shaft length and *z* is axial position along the element. The generalized lateral translation of the *i*th element at the axial position *z* is given by

$$\begin{bmatrix} U_{xi}(z,t) \\ U_{yi}(z,t) \end{bmatrix} = \begin{bmatrix} N_1 & 0 & N_2 & 0 & N_3 & 0 & N_4 & 0 \\ 0 & N_1 & 0 & -N_2 & 0 & N_3 & 0 & -N_4 \end{bmatrix} Q_i. \tag{2.4}$$

The lateral rotations about the x and y axes are given as

$$\Theta_x = \frac{\partial U_y}{\partial z}, \tag{2.5a}$$

$$\Theta_y = \frac{\partial U_x}{\partial z}. \tag{2.5b}$$

With the interpolated rotor element shape, the linearized dynamic equation for the *i*th element is given by

$$F_i = M_i \ddot{Q}_i + C_i \dot{Q}_i + \omega G \dot{Q}_i + K_i Q_i, \tag{2.6}$$

where M_i is the mass matrix, C_i is the damping matrix, G is the gyroscopic matrix, K_i is the stiffness matrix, and F_i is the generalized force vector. By defining the generalized displacement vector Q^T as $\dot{Q}_i$

$$Q^T = [\, q_1^T \; q_2^T \; q_3^T \; \dots \quad q_{n+1}^T]. \tag{2.7}$$

The rotor dynamic equation becomes

$$M_R \ddot{Q} + (D_R + \omega G_R)\dot{Q} + (K_R + \omega D_I + \dot{\omega} G_R + \omega^2 K_\omega) Q = F_R(t) \tag{2.8}$$

where $F_R(t)$ is the force vector defined in the radial direction, and ω is the rotational speed. Matrices M_R, K_R, and D_R represent the symmetric mass, stiffness, and damping matrices, respectively, G_R is the skew symmetric gyroscopic matrix, K_ω is the centrifugal stiffening matrix, and D_I is the rotating part of the internal damping matrix. Obviously, we can see in Equation (2.8) that the gyroscopic effect depends on the operating speed. The speed-dependent gyroscopic effect can introduce significant uncertainties to the control system designed for a constant operating speed, which affect the robustness and the performance of the system.

The general structure of the vector differential equation for a cylindrical undamped rotor can be rewritten as

$$\begin{bmatrix} M & 0 \\ 0 & M \end{bmatrix} \begin{bmatrix} \ddot{q}_x \\ \ddot{q}_y \end{bmatrix} + \omega \begin{bmatrix} 0 & G \\ G & 0 \end{bmatrix} \begin{bmatrix} \dot{q}_x \\ \dot{q}_y \end{bmatrix} + \begin{bmatrix} K & 0 \\ 0 & K \end{bmatrix} \begin{bmatrix} q_x \\ q_y \end{bmatrix} = \begin{bmatrix} F & 0 \\ 0 & F \end{bmatrix} \begin{bmatrix} u_x \\ u_y \end{bmatrix}, \tag{2.9}$$

where M is the mass matrix, G is the gyroscopic matrix, and K is the stiffness matrix. The lateral displacements in the x and y directions are given as u_x and u_y, respectively. The differential equation in (2.9) shows that the rotor dynamics in the x and y directions are only coupled by the gyroscopic effect, which is dependent on the rotor speed ω. The states of this differential equation correspond to the two lateral and the two angular degrees of freedom assigned to each node point. Therefore, the total number of states increases for rotors with complex geometries and large number of elements. A dynamic model with a large state vector is computationally intensive to simulate and thus leads to numerical problem during the design of the AMB rotor suspension controller. A common method of reducing the size of a state vector is to adopt the modal truncation approach, where the system equation (2.9) is transformed into the modal coordinates and irrelevant high frequency modes are discarded from the analysis. The transformation matrix transforms the rotor state vector from the physical coordinates to the modal coordinates by solving a generalized eigenvalue problem

$$K\,\phi = M\,\phi\,\lambda^2, \tag{2.10}$$

where the diagonal matrix λ is composed of the rotor resonant mode frequencies and the columns of the nonsingular matrix ϕ are vector mode shapes. The matrix ϕ is normalized such that

$$\phi^T\,M\,\phi = I, \tag{2.11a}$$

$$\phi^T\,K\,\phi = \lambda^2. \tag{2.11b}$$

Define new state vectors ζ_x and ζ_y following the coordinated transformation

$$\phi\, \zeta_x = q_x, \tag{2.12a}$$

$$\phi\, \zeta_y = q_y. \tag{2.12b}$$

Therefore, the modified dynamical equation yields the following form with the assumption $C_i = 0$

$$\phi^{\mathrm{T}} M \phi\, \ddot{\zeta}_x + \omega\, \phi^{\mathrm{T}} G \phi\, \dot{\zeta}_y + \phi^{\mathrm{T}} K \phi\, \zeta_x = \phi^{\mathrm{T}}\ \mathrm{F}\, u_x, \tag{2.13a}$$

$$\phi^{\mathrm{T}} M \phi\, \ddot{\zeta}_y + \omega\, \phi^{\mathrm{T}} G \phi\, \dot{\zeta}_x + \phi^{\mathrm{T}} K \phi\, \zeta_y = \phi^{\mathrm{T}}\ \mathrm{F}\, u_y, \tag{2.13b}$$

by substituting Equations (2.11a) and (2.11b) into (2.13a) and (2.13b), we obtain

$$\ddot{\zeta}_x + \omega\, G\, \dot{\zeta}_y + \lambda^2 \zeta_x = F_m\, u_x, \tag{2.14a}$$

$$\ddot{\zeta}_y + \omega\, G\, \dot{\zeta}_x + \lambda^2 \zeta_y = F_m\, u_y. \tag{2.14b}$$

The state space equation (2.14a) yields

$$\begin{bmatrix} \dot{\zeta}_x \\ \ddot{\zeta}_x \end{bmatrix} = \begin{bmatrix} 0 & I \\ -\lambda^2 & 2\zeta\lambda \end{bmatrix} \begin{bmatrix} \zeta_x \\ \dot{\zeta}_x \end{bmatrix} + \begin{bmatrix} 0 \\ F_m \end{bmatrix} f_x + \begin{bmatrix} 0 \\ \omega G \end{bmatrix} \zeta_y. \tag{2.15}$$

This can be simplified in the following form

$$\dot{x} = A\, x + B\, f_x + \omega \begin{bmatrix} 0 \\ G \end{bmatrix} \zeta_y, \tag{2.16}$$

therefore, the state space equation for the complete rotor lateral dynamics with the gyroscopic effect can be presented as

$$\begin{bmatrix} \dot{x} \\ \dot{y} \end{bmatrix} = \begin{bmatrix} A & \omega G_m \\ -\omega G_m & A \end{bmatrix} \begin{bmatrix} x \\ y \end{bmatrix} + \begin{bmatrix} B & 0 \\ 0 & B \end{bmatrix} \begin{bmatrix} f_x \\ f_y \end{bmatrix}. \tag{2.17}$$

where the combined force applied by the opposite coils of the AMB actuator in the x and y directions is given by f_x and f_y, respectively. G_m is the gyroscopic matrix after the coordinate transformation.

2.3.2 Modeling of AMB system

After modeling the rotor dynamics, we need to present a model of the AMB system and combine these two models to get the overall model for the rotor-AMB system. The displacement of the rotor supported by AMBs may be represented as

$$\begin{bmatrix} X_{amb1} \\ X_{amb2} \\ Y_{amb1} \\ Y_{amb2} \end{bmatrix} = \begin{bmatrix} C & 0 \\ 0 & C \end{bmatrix} \begin{bmatrix} x \\ y \end{bmatrix}, \tag{2.18}$$

where X_{amb} and Y_{amb} are the rotor displacements given at the AMB location in the x and y directions, respectively. Figure 2.9 shows a rotor that is supported by an AMB.

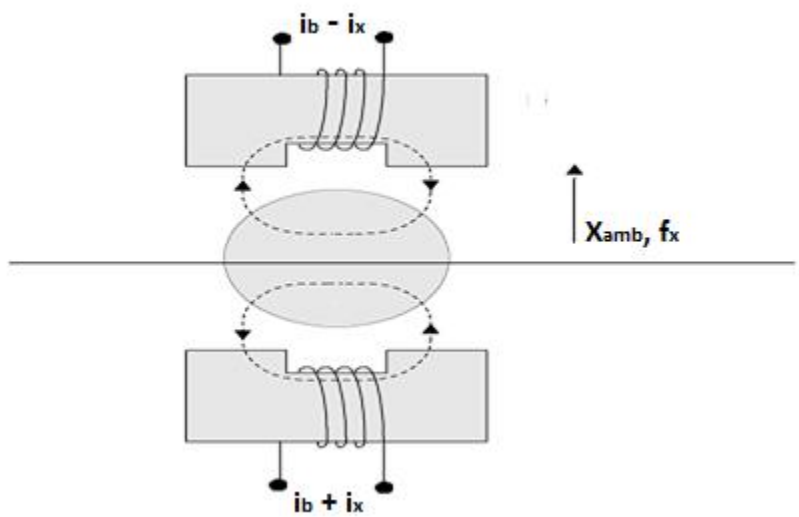

Figure 2.9 2D rotor-AMB system

As mentioned before, the AMBs generate a magnetic force to support the rotor in the axial and radial directions. These forces are functions of the rotor displacements and control currents and they can be represented by the following linearized equations

$$f_x = [\ K_x\ \mathrm{I}\ ]\ C + K_i \begin{bmatrix} i_{x1} \\ i_{x2} \end{bmatrix}, \tag{2.19a}$$

$$f_y = [\ K_x\ \mathrm{I}\ ]\ C + K_i \begin{bmatrix} i_{y1} \\ i_{y2} \end{bmatrix}, \tag{2.19b}$$

where K_x is the open loop stiffness, and K_i is the open loop current gain. The perturbation currents in the *x* and *y* directions are given by i_x and i_y, respectively.

2.3.3 Overall Assembly for Rotor-AMB system

By combining Equation 2.17, 2.19a, and 2.19b, we get the overall model of the rotor-AMB system which is given by the following equation

$$\begin{bmatrix} \dot{x} \\ \dot{y} \end{bmatrix} = \begin{bmatrix} A + BK_xC & \omega G_m \\ -\omega G_m & A + BK_xC \end{bmatrix} \begin{bmatrix} x \\ y \end{bmatrix} + \begin{bmatrix} BK_i & 0 \\ 0 & BK_i \end{bmatrix} \begin{bmatrix} i_x \\ i_y \end{bmatrix}. \tag{2.20}$$

2.4 Conclusions

In this chapter, we introduced the two main types of the compressor, the positive displacement and dynamic compressors, and how the pressure head is achieved in each type. In addition, some of the most popular problems in compressors such as rotating stall and compressor surge were discussed. Finally, we presented the modeling of the rotor-AMB system for the purpose of presenting control methods for them in the coming chapters.

Chapter 3

Control Theory

Generally, control theory can be approached from different directions. The first systematic techniques in control theory appeared in the 1930s. Control theory can be divided into two main parts: classical control and modern control. Classical control methods are based on either the root locus technique or compensator design in the frequency domain. Similar to the root locus technique, the modern control design methods were developed to deal with the placement of the closed-loop transfer function poles, in order to achieve the design specifications. For that, the state variables of the system have to be measured. In some cases, the state variables cannot be measured. Hence, we need to observe or estimate the system's state variables to be able to apply the state feedback. This can be done using a full-order state observer or a reduced-order state observer.

3.1 Linear Control Systems

In real life, most dynamic systems are nonlinear. The analysis and control of the systems with nonlinear dynamics are known to be difficult and complicated [7]. Because of that, linearization methods are used to get linear model approximations for these systems, which are easier to deal with. Generally, linear systems are divided into two main parts: linear time-varying (LTV) systems, where the outputs of the system depend on time, and linear time invariant (LTI) systems, where the system input-output characteristics do not change with time. An LTI system can be described in the time domain as a differential equation, and in the frequency domain as a transfer function. The general state space representation of a linear control system is given by

$$\dot{x} = A(t)\, x(t) + B(t)\, u(t), \tag{3.1}$$

$$y = C(t)\, x(t) + D(t)\, u(t), \tag{3.2}$$

where $x(t)$ is the n x 1 state vector, $u(t)$ is the r x 1 input vector, $y(t)$ is the p x 1 output vector, A is the n x n system matrix, B is the n x r input matrix, C is the p x n output matrix, and D is the p x r coupling matrix between the input and the output. In LTI systems, A, B, C, and D are constant matrices. The general solution of the LTI linear system state equation can be given as

$$x(t) = \Phi(t)\, x(0) + \int_0^t \Phi(t-\tau) B\, u(\tau) d\tau, \tag{3.3}$$

where $\Phi(t)$ is the state transition matrix, and it is given by $\Phi(t) = e^{At}$.

3.2 H_∞ Control

H_∞ Control is one of the most common techniques that are used to design advanced synthesis controllers. It achieves high levels of stability with a guaranteed performance for the systems. This control technique requires a good level of mathematical understanding for the dynamics of the system to design a controller with a good level of robustness against uncertainties and disturbances. The H∞ control method is used with unstructured uncertainties, which is the difference between the nominal and actual plant models [1]. The H∞ controller is designed based on an upper bound that includes all unmodeled uncertainties. Figure 3.1 shows an example for the upper bound in which all the unmodeled uncertainties stay below it.

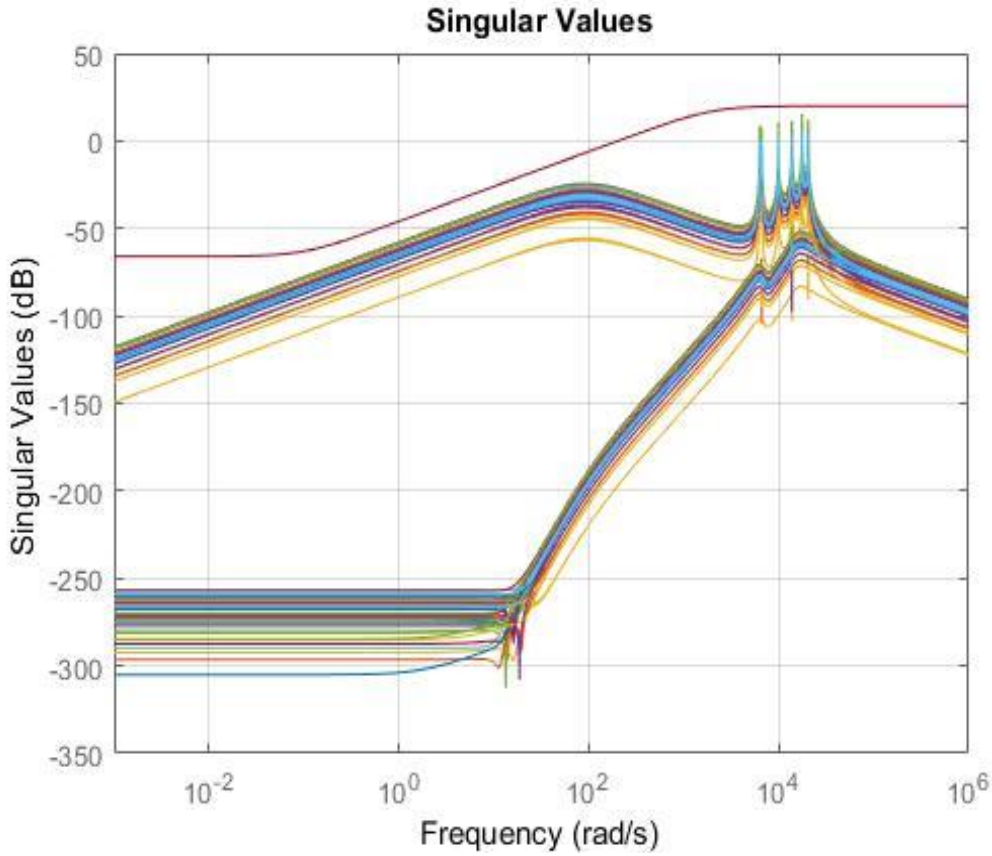

Figure 3.1 Example of an upper bound of unstructured uncertainties

The goal of the H_∞ control method is to design controllers that minimize the H_∞ norm of an augmented closed-loop transfer function. Generally, there are two main design methods for H_∞ controllers: loop shaping design and signal-based design. The loop-shaping technique is one of the widely used techniques to generate H_∞ controllers as it includes the performance requirements as performance weights in the early steps of the design process [10]. It is used to design multi-input multi-output (MIMO) controllers. In the loop shaping method, the closed-loop objectives are defined in terms of the specifications on the open loop singular values. On the other hand, the signal-based method represents design objectives through weighting functions on different inputs and outputs of the closed-loop system, and designs a controller that will minimize the H_∞ norm of

the augmented closed-loop transfer function [1]. A case study that compares between the loop-shaping and signal-based methods is presented in [11].

3.3 μ-Synthesis Control

The μ-synthesis method can be considered as an extended version of the H_∞ control method, where the systems' structured uncertainties are added to the design. Differently from the unstructured uncertainties, structured uncertainties are defined for particular parameters or characteristics of the controlled plant. The objective of the μ-synthesis method is to minimize the H_∞ norm of the closed-loop transfer function, and to maximize the level of the structured uncertainty that the system can deal with and remain stable. Figure 3.2 illustrates the interconnected system for the μ-synthesis method, where G(s) is the plant, *K*(s) is the controller, Δ(s) is the uncertainty in the plant model, and M(s) is the closed-loop transfer function of the system. The uncertainty Δ(s) and the plant G(s) are scaled, such that the maximum norm of Δ(s) equals 1.

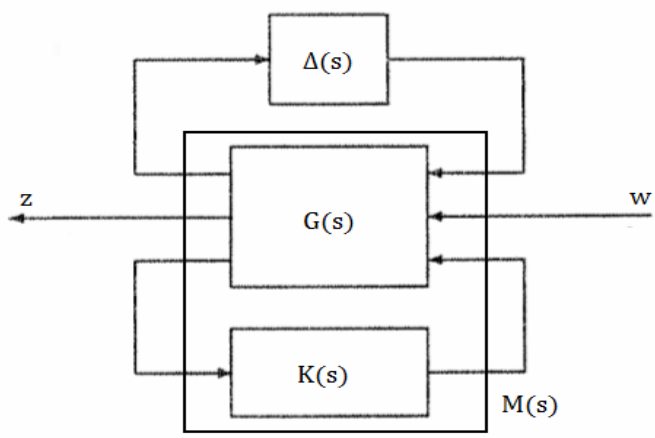

Figure 3.2 Interconnected system for μ-synthesis controller

The robust stability and robust performance of the closed-loop system M(s) can be measured through the Structured Singular Value (μ), which is defined as [12]:

$$\mu_{\Delta}(M) = \frac{1}{\min\{\sigma(\boldsymbol{\Delta}) : \boldsymbol{\Delta} \in \Delta, \det(I - M\Delta) = 0\}}, \tag{3.11}$$

where σ is the maximum singular value of the given matrix. We can see that the smallest value $\sigma(\boldsymbol{\Delta})$ in the set of all possible uncertainty Δ that makes det $(I-M\Delta) = 0$ is $1 / \mu_{\Delta}(M)$. This means that the interconnected loop is nonsingular to the given $\Delta(s)$ whenever $1 / \mu_{\Delta}(M) > 1$, and hence the interconnected system is stable.

3.4 Gain Scheduling Control

Over the last six decades, linear control methods have made important advancements in both theory and applications. Many applications in real world behave in a nonlinear manner, and their dynamics are approximated by linear models in order to apply linear controller design methods. On the other hand, there are some nonlinear systems, such as high performance aircrafts, that operate over a wide range of Mach numbers and altitudes, and the wide range of operation limits the accuracy of any single linearized model approximation. A common method that is used for the control of this class of nonlinear systems is to combine control laws that are specifically designed for different operating conditions along the system parameter range. This is the basic idea of the gain scheduling method.

3.4.1 Background

Gain scheduling is a control method that is used in nonlinear systems to optimize their performance. It is one of the most commonly used controller design approaches for nonlinear plants. This controller consists of a collection of linear controllers, each of which provides

satisfactory closed-loop stability and performance within different operating regions of the system. The operating region for the system is determined by a scheduling signal, also known as the scheduling variable, which may be either exogenous or endogenous with respect to the plant. Based on the characteristics of the scheduling signal, a controller is selected among the set of predesigned controllers. The gain scheduling method is suitable to use when the scheduling variable varies slowly compared to the control bandwidth.

The idea of gain scheduling first appeared in the 1960's. An early version of this technique was used in World War II to control the flight dynamics of rockets, in which the controllers were switched based on the measured altitude and other data. Gain scheduling attracted more attention after the introduction of linear parameter varying (LPV) systems in 1988 by Jeff. S. Shamma in his PhD dissertation [13]. The idea of the LPV systems is to represent nonlinearities of a system as a time varying parameters of a linear system. After Shamma's work, gain scheduling became one of the most common approaches to control nonlinear systems. The design of a gain scheduled controller can be described by three main steps [14]:

- The first step is to obtain a linear parameter-varying model for the nonlinear plant. Mainly, two approaches are used for this. The first approach is the Jacobian linearization of the nonlinear system around a set of equilibrium points of the plant, also called operating points, which leads to a family of linearized plants. The second approach is the quasi-LPV scheduling, where the plant's dynamics are represented to blind the nonlinearities as time-varying parameters that form the scheduling variables.
- The second step is to design a linear controller for each linear parameter-varying model that arises from the first step. This leads to a collection of linear controllers for a set of

scheduling variables. Interpolation may be considered to obtain the linear controllers corresponding to scheduling variables not included in the initial design.

- The third step is the main step in the implementation of the gain scheduled controller, where the controller's coefficients are scheduled based on the scheduling signals.

These steps can be clarified using the following example of a launching rocket in Figure 3.3, which is a highly nonlinear system. At the beginning or at the launching state, the point **a** represents the operating point of the system. As the rocket goes up, the operating point changes to point **b**. As the rocket goes further, the operating point changes to **c** and so on. What gain scheduling control involves is to find linear approximation models of the system around each operating point and design a linear controller for each linear model of the system. A scheduling signal based on the measured state of the rocket determines the operating point of the system, and the appropriate controller to switched on.

Gain scheduling methods can be classified in different ways according to the decomposition of the original system dynamics, the classification of the input/output signals, and the method used for the design of the linear control law. Gain scheduling method may be classified based on how the nonlinear dynamics of the plant are decomposed. The gain scheduling control method may:

- decompose the nonlinear problem into linear sub-problems, or
- decompose the nonlinear problem into non-linear sub-problems.

Based on the properties of the input/output signals, gain scheduling methods may also be divided into:

- continuous gain scheduling methods,

- discrete gain scheduling methods, or
- hybrid or switching gain scheduling.

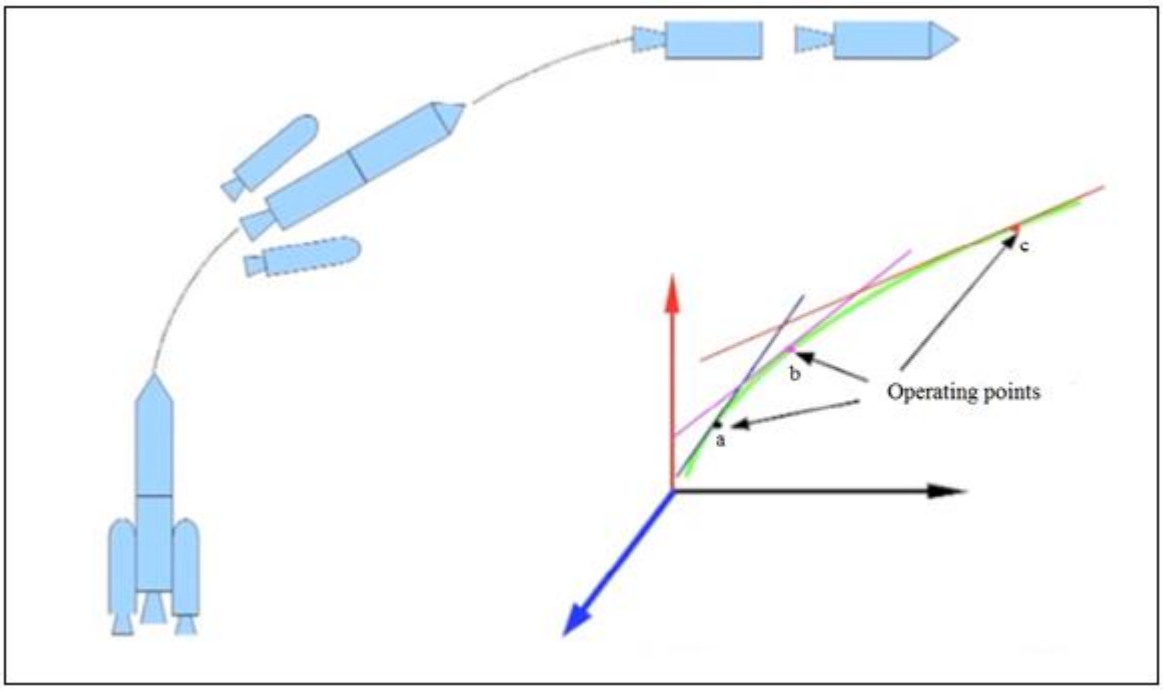

Figure 3.3 Launching rocket

Finally, based on the design method used for the linear control law, gain scheduling can be divided into:

- classical control-based gain scheduling,
- Lyapunov approach-based gain scheduling synthesis,
- linear fractional transformation (LFT) formulation-based gain scheduling synthesis, or
- fuzzy control gain scheduling.

The classical control-based gain scheduling incorporates methods in classical control to design the collection of linear controllers. Classical control methods require linear approximations

of the nonlinear plant around a family of static operating points [18]. Lyapunov approach and LFT synthesis techniques are based on LPV or LFT representation of the plant, respectively. These methods yield improved performance, robustness, and stability when compared to the classical method.

One of the main concerns while switching between the controllers is to achieve a smooth transfer between them. High transient vibrations could occur when switching between the controllers, which degrades the robustness and stability of the closed-loop system. Generally, there are two main techniques for bumpless transfer between the controllers: the conditioning technique [15] and the observer based technique [16]. The idea of the conditioning technique is to match the input signal of the offline controller with the output signal of the online controller. In other words, the states of the offline controller are changed based on the measurements of the online controller signal. This results in a fast return to the reference signal (online signal), and the smooth transfer between the controllers is guaranteed. In the observer based technique, the initial conditions of the off-line controller are estimated in order to guarantee the continuity in the controller output signal at the switching time.

3.4.2 Linear Parameter Varying Systems

As mentioned before, the gain scheduling technique became more popular after the introduction of linear parameter varying systems by Shamma [13] in 1988. In the gain scheduling method, a controller is built for a nonlinear system by gathering a set of linear controllers to cover the whole operating range. The switching between these controllers is based on the scheduling signals (also called scheduling variables). The nonlinear plant dynamics are represented as a parameterized linear system. The linear parameter varying (LPV) system is represented as

$$\dot{x} = \mathrm{A}(\Theta)\, x + \mathrm{B}(\Theta)\, u, \tag{3.12a}$$

$$y = C(\Theta)\, x. \tag{3.12b}$$

where Θ is an exogenous parameter. The LPV framework is considered as an interface between the linear and the nonlinear dynamics of the system [27].

3.4.3 Active Magnetic Bearings and Gain Scheduling Control

In rotor-AMB systems, the rotor is unstable; therefore, it needs to be stabilized using active feedback control. The rotor-AMB systems' dynamics are affected by many factors such as the nonlinearities, external disturbances, and model uncertainties. Many robust optimal control methods are used to stabilize rotor-AMB systems such as H_∞ method, μ-synthesis, and H_2 control technique. H_∞ control methods are used to synthesize controllers that achieve stabilization with guaranteed performance. The goal of the H_∞ control method is to design controllers that minimize the H_∞ norm of an augmented closed-loop transfer function [1]. The μ-synthesis method can be considered to be an extended version of the H_∞ control method, where the systems' structured uncertainties are added to the design. Differently from the unstructured uncertainties, structured uncertainties are defined for particular parameters or characteristics of the controlled plant. The objective of the μ-synthesis method is to minimize the H_∞ norm of the closed-loop transfer function, and to maximize the level of the structured uncertainty that the system can deal with and remain stable.

Switching amplifiers are commonly used in AMBs. However, their power supply has a finite supply voltage, which limits the maximum AMB force slew rate. A bias current can be introduced to improve the force slew rate of the AMB system, but this may result in AMB losses due to the eddy currents and the hysteresis effects. Also, it may result in rotor heating due to the added power dissipated by the AMBs. A gain scheduled control with a low bias current was presented in [25] to control AMBs. The nonlinear system dynamics were formulated as a quasi-

LPV system, and gain scheduled H∞ controllers were synthesized. The plant and the controller were presented into the LFT form for the robustness analysis with linear time varying uncertainties and multiplicative linear time invariant uncertainties. The robustness analysis consisted of finding an upper bound to the structured singular value of the closed-loop system using iteration between two minimizations, the μ analysis problem and the L_2 gain problem. The robustness analysis showed that the gain scheduled controller provided little robustness to the closed-loop system.

Imbalance in rotating machines leads to synchronous vibrations due to the generated unbalance forces. Many solutions have been proposed for this problem, but most of them are designed for magnetic bearings that operate at a single speed. Gain scheduled controllers are better suited to handle variable speed cases because the frequency of vibration varies with the operating speeds. Gain scheduled H_∞ controllers have been used for this problem [33]. However, as the operating speed increases, the order of the controller also increases in order to satisfy stricter performance objectives. This is due to the need of higher order weighting functions in the controller synthesis, which also increases the order of the controller. High order controllers may be difficult to implement in practical applications. Another approach was presented in [26] using a discrete-time gain scheduled *Q*-parameterization controllers. As the frequency of the vibrations is equal to the rotational speed, the free parameter *Q* of the *Q*-parameterization controller is scheduled as a function of the rotational speed. The authors of [26] showed that satisfactory robust stability and the disturbance rejection capabilities were achieved by the closed-loop system for the entire operating speed range of the AMB.

Generally, the lateral dynamics of AMBs are decoupled for low rotating speeds. The shaft axis of rotation is always aligned with the bearing center line, hence the inertia-induced moments on the disk are neglected. But when magnetic bearings are subjected to a continuous increment in

the operating speed, the shaft rotational axis start to diverge from the bearing's center line due to the rotor gyroscopic effects [1]. The speed-dependent gyroscopic effect can introduce significant uncertainties to the control system designed for a constant operating speed. Gain scheduled controllers were used to solve this problem using different synthesis techniques. In [17], the LPV gain scheduling, with fixed and parametric Lyapunov functions, and the LFT gain scheduling were applied to two types of flywheel rotors: drum type and disk type. The author evaluated these synthesis techniques from different perspectives such as performance, robustness, implementation, and the computation complexity of these approaches.

3.4.4 Advantages and Disadvantages of Gain Scheduling Method

The main advantage of the gain scheduling technique is that we can use linear design methods for nonlinear systems. In other words, linear control tools including output feedback methods, time domain techniques, and frequency domain techniques can be used for nonlinear systems. Also, systems that operate under the gain scheduling control respond quickly to changes in operating conditions [13].

On the other hand, the gain scheduling technique has some disadvantages. The main disadvantage is a result of using linear control methods, which may results in a local stability of the system around the operating point. In addition, as the gain scheduling technique depends on the scheduling variables, an improper selection of these variables may affect the performance of the controller. Therefore, the scheduling variables must be selected properly in order to reflect the changes in the system's dynamics when operating conditions change. Finally, gain scheduling is an application specific method in which the selection of the scheduling signal can vary from system to system. For example, some control applications may not have an accessible scheduling signal that can be used to design the control law.

3.5 Conclusion

This chapter presents a brief introduction to linear control systems and some advanced synthesis controller design methods in linear systems, such as the H_∞ control and μ-synthesis control methods. Generally, the H_∞ control method is used to design controllers for systems that have unstructured uncertainties, whereas the μ-synthesis control method is used for the systems with structured uncertainties. These optimal control methods are commonly used in cases where the proportional-integral-derivative (PID) controllers are not able to achieve the design requirements. In addition, we discussed the gain scheduling control method, which is one of the most popular methods that are used to optimize the performance of nonlinear systems. In addition, some of the common control challenges of rotor-AMB systems were presented, and we discussed how the gain scheduling control was applied to solve them in the literature. Furthermore, some of the main advantages and disadvantages for the gain scheduling control technique were discussed.

Chapter 4

Gain-Scheduled Control for Rotor-AMB System

In this chapter, we will present a case study of the gain scheduling control method applied to a rotor-AMB system. In particular, the μ-synthesis based gain scheduling technique is used to design an AMB levitation controller for a prototype motor that covers an operating speed range between 0 and 50,000 rpm. For the implementation of the gain scheduling technique, this speed range was divided into three regions, and a μ-synthesis controller was designed for each region. Furthermore, an observer-based bumpless transfer technique was implemented to switch between these controllers.

4.1 Rotor-AMB System Model

The test rig that is considered here consists of a flexible rotor with an integrated motor core. This rotor is supported horizontally by two radial AMBs and axially by a single thrust AMB. The assembled rotor weighs 390.2 pounds, with a total length of 52 inches, and the diameter varies between 3.54 and 11.3 inches. Figure 4.1 illustrates a FEM mesh of the rotor with the sensor locations and the AMB locations. The operating speed range under which the system is tested is between 0 and 50,000 rpm. Table 5.1 illustrates the natural frequencies of the test rig rotor.

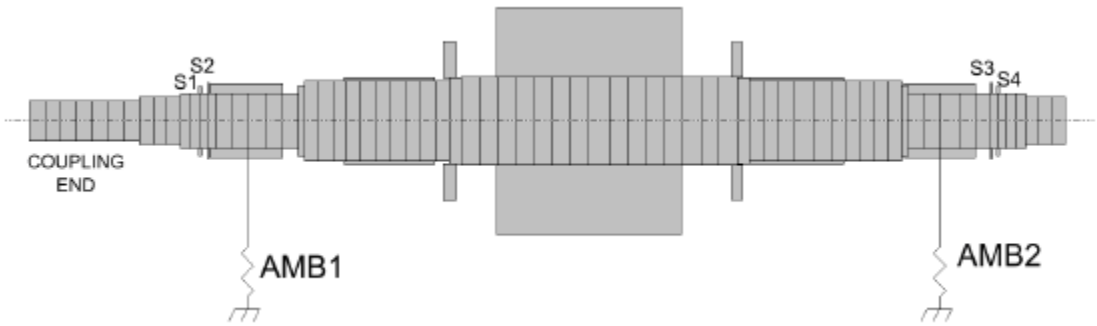

Figure 4.1 FEM mesh of the rotor

Table 4.1 Natural frequencies of the test rig rotor

List of modes	ω_n (Hz)
1st bending mode	270.82
2nd bending mode	331.38
3rd bending mode	745.05

In this study, uncertainties in the modal frequency, modal damping, and the rotating speed of the shaft were considered. The uncertainty in the modal frequency/damping of the rotor was captured by a complex-valued uncertainty in the pole location of the open-loop AMB system. This can be represented as a circular uncertainty region in the complex plane that contains the nominal pole and has a radius of ±5% of the mode frequency. The uncertainty region is shifted to the left to avoid crossing the imaginary axis. The defined uncertainty region for the pole location is illustrated in Figure 4.2.

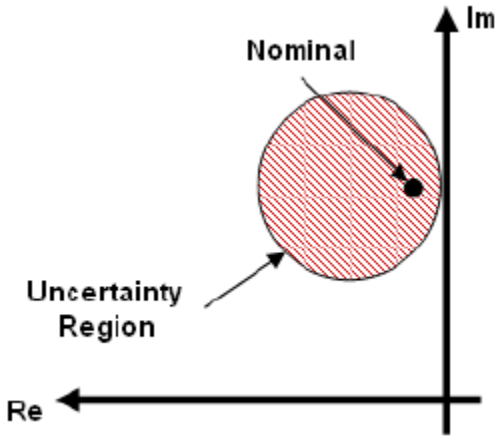

Figure 4.2 Pole location according to the uncertain rotor mode.

4.2 Gain-Scheduled Controller Design

After defining the uncertainties of the plant, an interconnected system is built for the μ-synthesis design. Figure 4.3 represents the 4-block interconnected system that was used in this study where P is the transfer function of the system and K is the feedback controller. The functions *Wi* for *i* from 1 to 4 are the weighting functions for the controller. The inputs to the interconnected system are the weighted noise input w_1, the weighted disturbance input w_2, and the control input u. The outputs of the system are the weighted control signal z_1, the weighted controller input z_2, and the control output y.

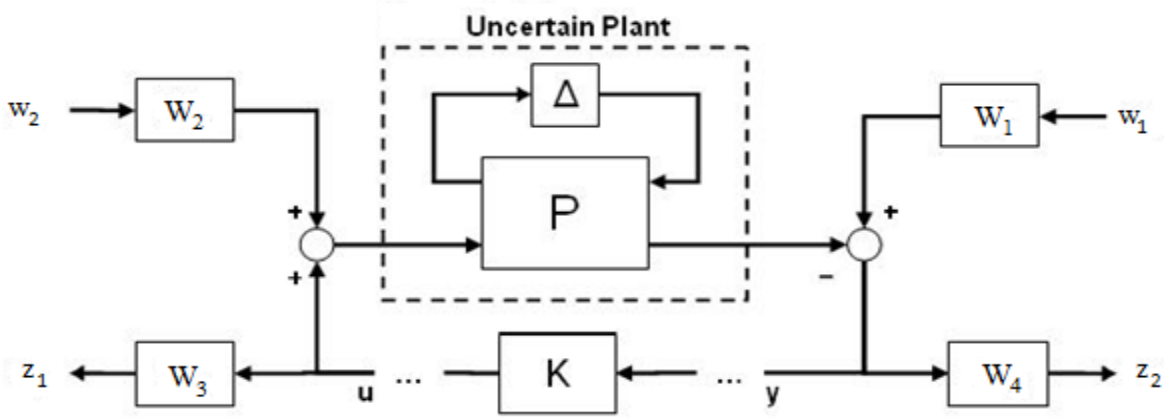

Figure 4.3 The interconnected system for μ-synthesis

From the interconnected system in Figure 4.3, the μ-synthesis controller is found for the feedback loop. For the nominal system with Δ = 0, the relationship between the performance defining inputs and outputs, w_i and z_i, are given by the following matrix of transfer functions

$$\begin{bmatrix} z_1 \\ z_2 \end{bmatrix} = \begin{bmatrix} W_3(I-KP)^{-1}KW_1 & W_3(I-KP)^{-1}W_2 \\ W_4(I-KP)^{-1}W_1 & W_4(I-KP)^{-1}PW_2 \end{bmatrix} \begin{bmatrix} w_1 \\ w_2 \end{bmatrix} \tag{4.1}$$

The transfer functions of the above matrix describe the different desired performance characteristics of the nominal closed-loop system. The weighting functions, $W_1,\ W_2,\ W_3,$ and W_4, were selected based on the performance requirements of the closed-loop system. Weighting function W_1 was selected to limit the bandwidth of the feedback controller, W_2 is defined to set the minimum disturbance rejection requirement, and W_4 is selected to limit the output sensitivity function. The resulting weighting functions are:

$$W_1 = \frac{1.5(s+10^3)}{s+10^5}I,\ W_2 = \frac{1}{4}I,\ W_3 = I,\ W_4 = \frac{1}{3}I. \tag{4.2}$$

As mentioned before, the modal frequency, the modal damping, and the rotating speed of the shaft were considered to be time-varying uncertainties. The operating speed range was divided into three regions, defined between 1) 0 to 18,000 rpm, 2) 17,000 to 34,000 rpm, and 3) 33,000 to 50,000 rpm. For each region, a μ-synthesis controller was designed to satisfy the robustness and the performance requirements. An overlap was included between the speed regions in order to guarantee the stability at the switching points. For the first region, the derived controller has 284 states, which was later reduced to 60 states using model reduction techniques based on the Hankel singular value. Figure 4.4 illustrates the Hankel Singular Value plot for the μ controller of the first region.

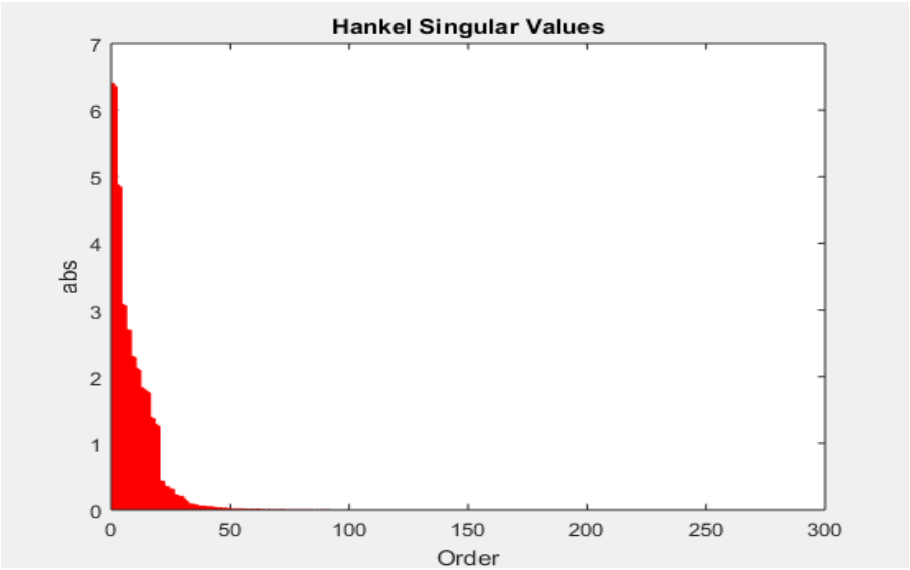

Figure 4.4 Hankel Singular Value plot for the μ controller of the first region

Figure 4.5 shows the robust performance μ value obtained for the closed-loop system within the first operating speed region. We can see that the μ value is less than 1 for all frequencies. Similar results were obtained for the remaining speed regions, which indicate that the robust stability and robust performance objectives have been achieved.

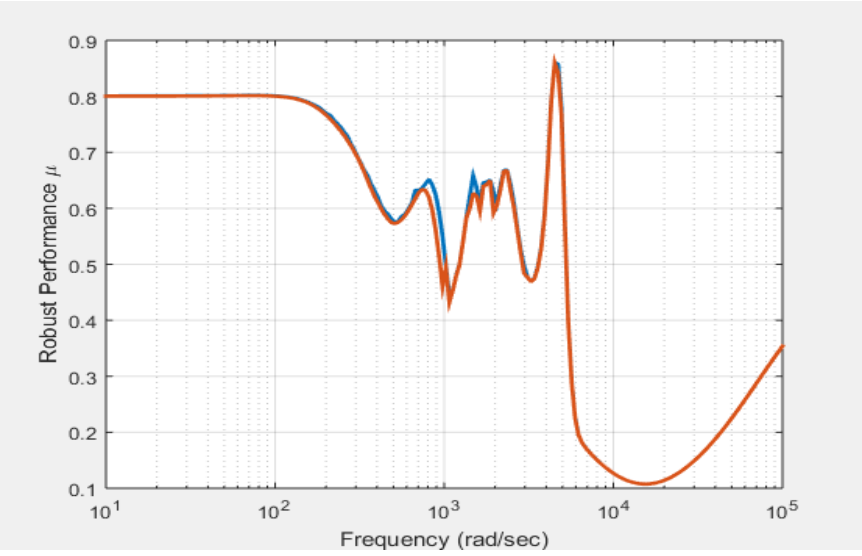

Figure 4.5 μ value of the interconnected system for the first region

In order to achieve a smooth transfer between the controllers in different speed regions, we implemented an observer based bumpless transfer technique. The state space representation of the i_{th} controller equations can be represented as

$$\dot{\eta}_i(t) = A_{c,i}\, \eta_i(t) + B_{c,i}\, y(t) + \xi_i(t), \tag{4.3}$$

$$u_i(t) = C_{c,i}\, \hat{\eta}(t) + \Theta_i(t). \tag{4.4}$$

where $y(t)$ and $u(t)$ are the online controller input and output, respectively. $\xi_i(t)$ and $\Theta_i(t)$ are assumed to be white Gaussian noise with zero mean. The observer generates $\hat{u}_i(t)$ and $\hat{\eta}_i(t)$ by the observer dynamic equation:

$$\dot{\hat{\eta}}_i(t) = A_{c,i}\, \hat{\eta}(t) + B_{c,i}\, y(t) + K_i\, [\, u(t) - C_{c,i}\, \hat{\eta}_i(t)], \tag{4.5}$$

$$\hat{u}_i(t) = C_{c,i}\, \hat{\eta}_i(t). \tag{4.6}$$

The Kalman filter gives the optimal estimate of the initial states in terms of the mean square error [19]. It is noted that the observer equation is similar to the controller, with a correction term added to the observer based on the error between the actual and estimated output. In the implementation of the bumpless transfer technique, the controller corresponding the current operating speed region is online. The remaining controllers are operated in the offline "observer" mode as represented in Equations (4.5) and (4.6). If the closed-loop system transitions from one operating region to the next, the controller corresponding to the new speed region becomes online, and the remaining control laws are switched to the observer mode.

The observer gains used in the bumpless transfer method were obtained by following the Linear Quadratic Regulator (LQR) design method. It can be demonstrated that the observation error corresponding the Equation (4.5) and (4.6) approaches zero if the dual system

$$\dot{\bar{\eta}}_i = A_{\mathrm{c,i}}^{\mathrm{T}} \bar{\eta}_i + C_{\mathrm{c,i}}^{\mathrm{T}} \nu(t), \quad \nu(t) = K_i^{\mathrm{T}} \bar{\eta}, \tag{4.7}$$

is stabilized. The LQR method provides the gain K_i^{T} such that the closed-loop system minimizes the quadratic objective function

$$J = \int_{-\infty}^{\infty} (\bar{\eta}^{\mathrm{T}} Q \bar{\eta} + \nu^{\mathrm{T}} R \nu) \mathrm{d}t, \tag{4.8}$$

The matrix Q is then the weight on the states' energy, and R is the weight on the input energy.

4.3 Simulation Results

The performance of the AMB system under the gain scheduling control law was tested in simulation in the presence of rotor unbalance weights. Unbalance weights were added based on the specification of the API standard 541, in which the standard input unbalance in gram-mm for the forced response analysis of rotordynamic systems is set as

$$U_{\mathrm{b}} = 6350 W/N, \tag{4.9}$$

where W is the journal static load in kg, and N is the maximum rotational speed in rpm. In our simulation, we used two unbalance weights of $10U_{\mathrm{b}}$. One unbalance was added to each balancing plates of the rotor, separated by 180 degrees in phase.

For the simulation test, the rotor was ramped up from 0 to 50,000 rpm. Figure 4.6 and Figure 4.7 show the rotor orbit at the sensor locations S_2 and S_3, respectively. Figure 4.8 shows the maximum rotor vibration level at the sensor locations over the speed range for the unbalance test. The simulation results show that the vibration level is maintained within an acceptable level, and it varies gradually along the speed range, as it is shown in Figure 4.8. Also, the smooth transfer was achieved when switching between the controllers.

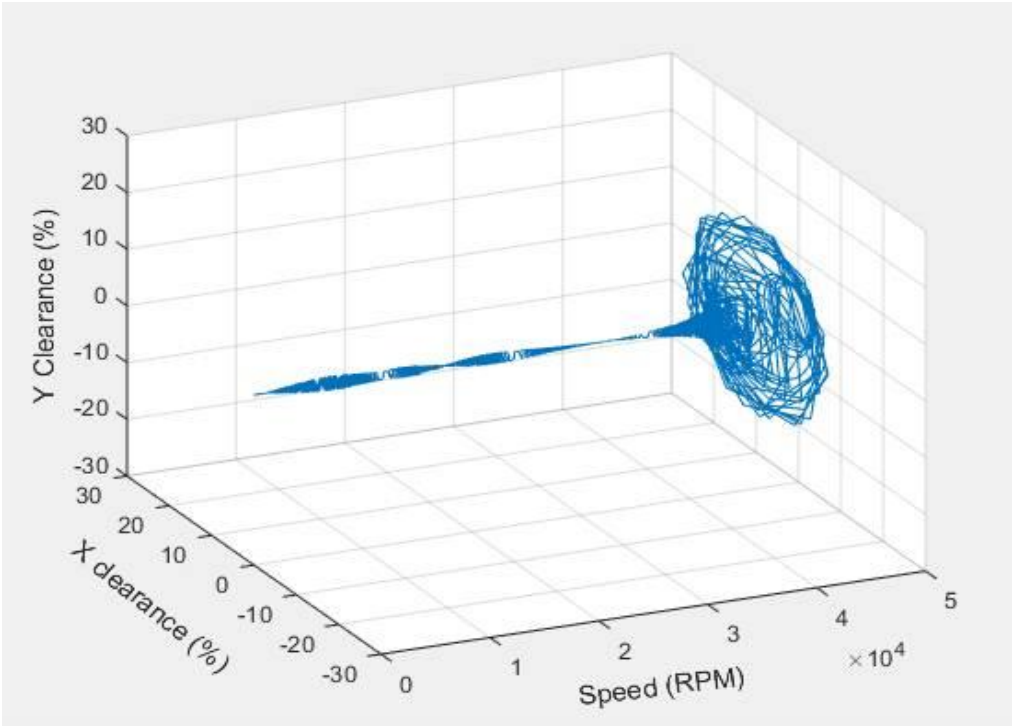

Figure 4.6 Rotor orbit at sensor S2 location over the speed range

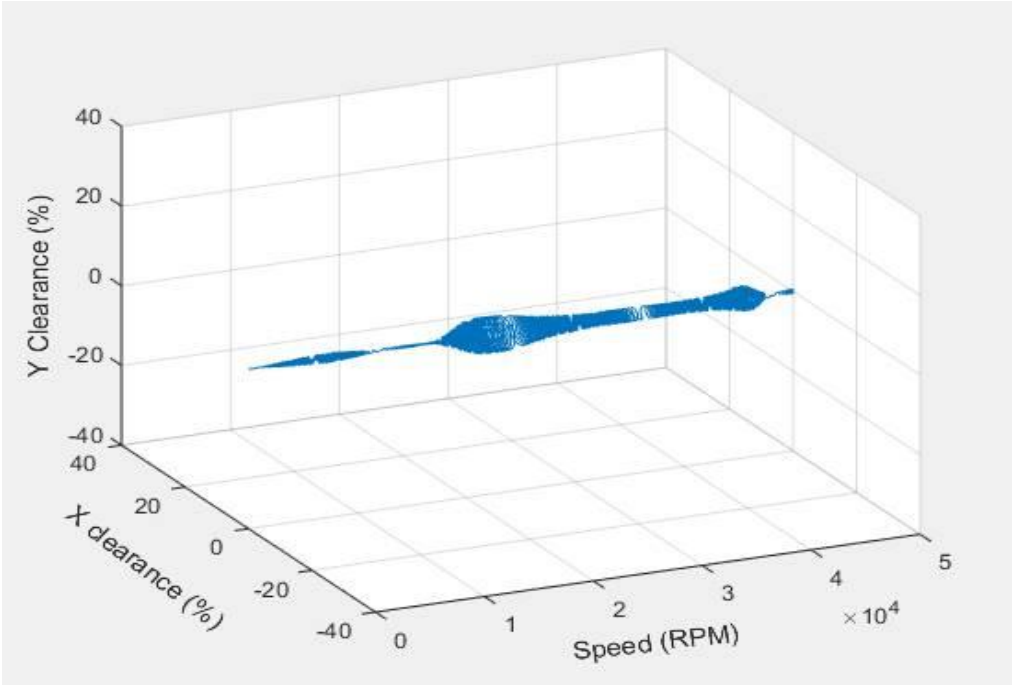

Figure 4.7 Rotor orbit at sensor S3 location over the speed range

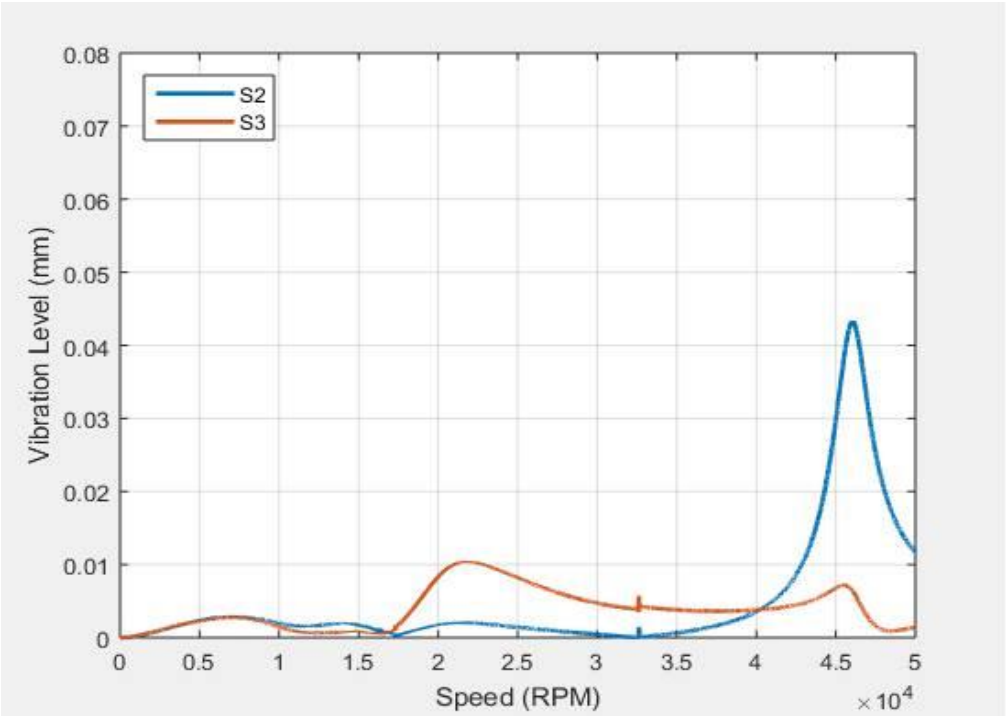

Figure 4.8 Rotor unbalance response

4.4 Conclusion

In this chapter, a μ-synthesis based gain scheduling technique was used to design a levitation controller for a prototype motor with AMBs. The operating speed range of the motor was divided into three regions, and a μ-synthesis controller was designed for each region. Both the design and simulation test results showed that robust performance was achieved, and rotor vibration was within an acceptable level for the entire operating speed range. An observer-based bumpless transfer scheme was implemented in our simulation to achieve smooth switching between the gain-scheduled controllers.

Chapter 5

Gain-Scheduled Controller for Compressor Surge

In this chapter, we will introduce the work in [1] for a compressor surge control in an AMB supported compression system using H_∞ control technique. Then, we will extend this work by implementing the gain scheduling technique to design a surge control law that extends the stable operating region of the compressor. This chapter will be organized as the following. First, we will introduce the compression system model and the surge controller design in [1]. After that, the design of the gain-scheduled controller will be presented. Finally, we will present simulation results to illustrate the effectiveness of the gain-scheduled surge controller.

5.1 Compression System Model

It is important to model the compression system properly in order to design a controller that is able to stabilize the system with a good level of robustness. One of the most popular models that is used to represent compression systems for surge control is the Greitzer model [28]. This model combines the dynamics of the compressor, the plenum volume, and the throttle valve in order to capture the surge instability. Compared to other compression system models, the Greitzer model adds the transient dynamics of the system over the known steady state characteristics, thus allowing for simpler model equations. This model represents the non-dimensional mass flow rate Φ and pressure rise Ψ as

$$\Phi = \frac{m}{\rho_{01} U A_c}\,, \tag{5.1}$$

$$\Psi = \frac{\Delta P}{\frac{1}{2}\rho_{01}U^2}\ , \tag{5.2}$$

where m is the dimensional mass flow rate, $\rho_{01}$is the gas density in the ambient condition, U is the impeller tip speed, A_c is the cross section area of the compressor duct, and ΔP is the dimensional pressure rise. The Greitzer model of the compression system in terms of the non-dimensional mass flow rate and pressure rise is given by

$$\frac{d\Phi_c}{dt} = \mathrm{B}\ \omega_H(\Psi_c - \Psi_p), \tag{5.3a}$$

$$\frac{d\Phi_{th}}{dt} = \frac{\mathrm{B}\ \omega_H}{G}(\Psi_p - \Psi_{th}), \tag{5.3b}$$

$$\frac{d\Psi_p}{dt} = \frac{\omega_H}{G}(\Phi_c - \Phi_{th}), \tag{5.3c}$$

$$\frac{d\Psi_c}{dt} = \frac{\omega_H}{\tilde{\tau}}(\Phi_{c,ss} - \Phi_c), \tag{5.3d}$$

where Φ_c and Φ_{th} are the compressor mass flow rate and the throttle valve mass flow rate, respectively. Ψ_p is the plenum pressure rise and Ψ_c is the compressor pressure rise. B represents the Greitzer stability parameter and $\tilde{\tau}$ represents the compressor time constant. G is a parameter that depends on the ratio between the compressor and throttle duct dimensions. ω_H is the Helmholtz frequency and it is given by

$$\omega_H = a_{01}\sqrt{\frac{A_c}{V_p\,L_c}}\ , \tag{5.4}$$

where a_{01} is the speed of sound at ambient condition, A_c is the area of the compressor duct, V_p is the volume of the plenum, and L_c is the length of the compressor. The compression system model is built based on the steady state characteristics of the flow [1]. The non-dimensional steady state compressor pressure rise is a function of the compressor mass flow rate, and it is given as

$$\Psi_{c,ss}(\Phi_c) = A_1\, \Phi_c^3 + B_1\, \Phi_c^2 + D_1, \tag{5.5}$$

where the coefficients A_1, B_1, and D_1 are determined using the third order polynomial fitting that was presented in [32] to determine the curve from the measurements of the steady-state pressure and mass flow rate of the compression system.

This model can be considered as a good start from which we can study the control of the compressor surge instability. However, Greitzer model has a disadvantage of not including the pipeline dynamics based on assumptions that the gas or fluid velocity in the plenum volume is negligible and the pressure distribution is uniform. This is not true in many compression systems. We will talk about the pipeline modeling later in this section.

Assuming that the throttle valve flow dynamics are negligible and $\tilde{\tau}$ is small, the mathematical model of the compression system reduced to three main parts: the compressor, the pipeline, and the plenum volume. The compressor and plenum dynamic equations are given as

$$\dot{\Phi}_c = B\, \omega_H \left(\Psi_{c,ss}\,(\Phi_c) + \frac{P_{01}}{\frac{1}{2}\rho_{01}\, U^2}\, k_{cl}\, \delta_{cl} - \Psi_p\right), \tag{5.6a}$$

$$\dot{\Psi}_p = \frac{\omega_H}{B}\,(\Phi_c - \Phi_p). \tag{5.6b}$$

where $k_{cl}$is the tip clearance gain, and δ_{cl} is the impeller tip clearance that can be actuated from the AMBs of the compressor. P_{01} is the inlet absolute pressure. The plenum mass flow rate Φ_p will come from the pipeline equation. More details about the equations' derivation can be found in [1].

Pipeline modeling techniques were proposed by Goodson [29], and Krus et al. [30]. The authors of [1] used the model that was proposed by Krus et al. and studied the best position to implement the pipeline model in the compression system model. The pipeline model was located

at the compressor exhaust (between the compressor and the plenum volume), and at the plenum volume output (between the plenum volume and the throttle valve). The idea was to compare and match the experimental and simulation results for the Bode plot of the transfer function from the tip clearance (δ_{cl}) to the plenum volume pressure rise. The results showed that the best place to locate the pipeline acoustic model was at the plenum volume output. Figure 5.1 shows the block diagram of the compression system model with the added pipeline model at the plenum volume output.

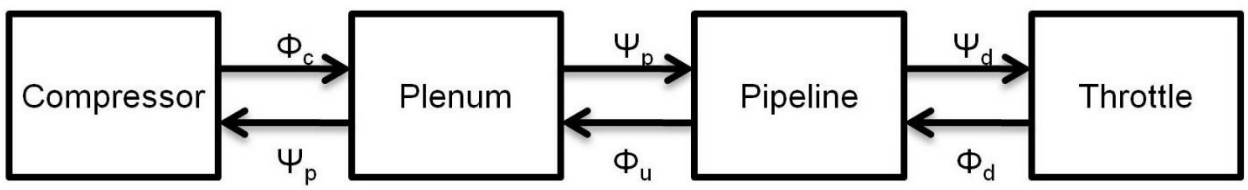

Figure 5.1 Block diagram of the compression system with the added pipeline model [1]

The resulting state space representation of the pipeline model with the non-dimensional variables is given as

$$\begin{bmatrix} \dot{\Psi}_{th} \\ \dot{\Phi}_p \end{bmatrix} = \begin{bmatrix} 0 & \frac{2\,A_{12}\,A_c}{\rho_u\,U} \\ \frac{A_{21}\,\rho_u\,U}{2\,A_c} & A_{22} \end{bmatrix} \begin{bmatrix} \Psi_{th} \\ \Phi_p \end{bmatrix} + \begin{bmatrix} 0 & \frac{2\,B_{12}\,A_c}{\rho_u\,U} \\ \frac{B_{21}\,\rho_u\,U}{2\,A_c} & B_{22} \end{bmatrix} \begin{bmatrix} \Psi_p \\ \Phi_{th} \end{bmatrix} +$$

$$\begin{bmatrix} 0 \\ \frac{\rho_u\,P_{01}}{\rho_{01}\,U\,A_c}\,(A_{21} + B_{21}) \end{bmatrix}, \tag{5.7}$$

where ρ_u is the density of the gas in the pipline. A_{ij} and B_{ij} are coefficient matrices of the state space representation of the pipeline dynamics. More details on the calculations of these coefficients can be found in [1].

In the throttle valve, assuming subsonic flow conditions, the non-dimensional mass flow rate is a function of the plenum pressure rise and the throttle percentage opening u_{th}, and it is given by

$$\Phi_{th} = c_{th}\, u_{th} \sqrt{\Psi_{th}}, \tag{5.8}$$

where c_{th} is the valve constant. Finally, the complete compression system equations are

$$\dot{\Phi}_c = B\, \omega_H \left(\Psi_{c,ss}(\Phi_c) + \frac{P_{01}}{\frac{1}{2}\rho_{01} U^2} k_{cl}\, \delta_{cl} - \Psi_p\right), \tag{5.9a}$$

$$\dot{\Psi}_p = \frac{\omega_H}{B}(\Phi_c - \Phi_p), \tag{5.9b}$$

$$\dot{\Psi}_{th} = \frac{2\, A_{12}\, A_c}{\rho_u\, U}\Phi_p + \frac{2\, B_{12}\, A_c}{\rho_u\, U} c_{th}\, u_{th} \sqrt{\Psi_{th}}\,, \tag{5.9c}$$

$$\dot{\Phi}_p = \frac{A_{21}\, \rho_u\, U}{2\, A_c}\Psi_{th} + A_{22}\Phi_p + \frac{B_{21}\, \rho_u\, U}{2\, A_c}\Psi_p + B_{22}\, c_{th}\, u_{th}\sqrt{\Psi_{th}} + \frac{\rho_u\, P_{01}}{\rho_{01}\, U\, A_c}(A_{21} + B_{21}). \tag{5.9d}$$

Table 5.1 shows the values of the parameters of the theoretical model as in [1].

Table 5.1 Model parameters for the compression system

Parameter	**Symbol**	**Unit**	**Value**
Comp. duct length	L_c	m	1.86
Comp. duct cross area	A_c	m^2	0.0082
Corrected A_1 coeff.	A_1	-	-172.6
Corrected B_1 coeff.	B_1	-	36.88
Corrected D_1 coeff.	D_1	-	1.029

Design tip clearance	cl_n	mm	0.6
Greitzer stab. parameter	B	-	0.44
Helmholtz frequency	ω_H	rad/s	80.1
Impeller tip speed	U	m/s	213.24
Impeller blade height	b_2	mm	8.21
Inlet pressure	p_{01}	pa	101,325
Inlet gas density	ρ_{o1}	kg/m^3	1.165
Plenum volume	V_p	m^3	0.049
Pipeline length	L	m	6.5
Throttle constant	c_{th}	-	1.7197
A_{12} coeff.	A_{12}	-	3.7 * 10^6
A_{21} coeff.	A_{21}	-	-0.0019
A_{22} coeff.	A_{22}	-	-8
B_{12} coeff.	B_{12}	-	-3.7 * 10^6
B_{21} coeff.	B_{21}	-	0.0019
B_{22} coeff.	B_{22}	-	7.98

5.2 Compressor Surge Controller Design

After deriving the dynamic equations for the compression system, the authors of [1] designed the stabilizing controller for compressor surge using the impeller tip clearance as

actuation through the AMB. They used the H_∞ control method to design the stabilization controller. This requires the linearization of the compression system model. They introduced new state variables as the difference between the original state variables and their corresponding equilibrium value at the linearization point. The equilibrium point is the intersection point between the compressor characteristic curve and the load curve at a given speed. The speed of 16290 rpm was chosen to be the operating speed, and the throttle valve opening of 17% was chosen for the linearization point. Figure 5.2 shows the characteristic curve for the compressor at different operating speeds.

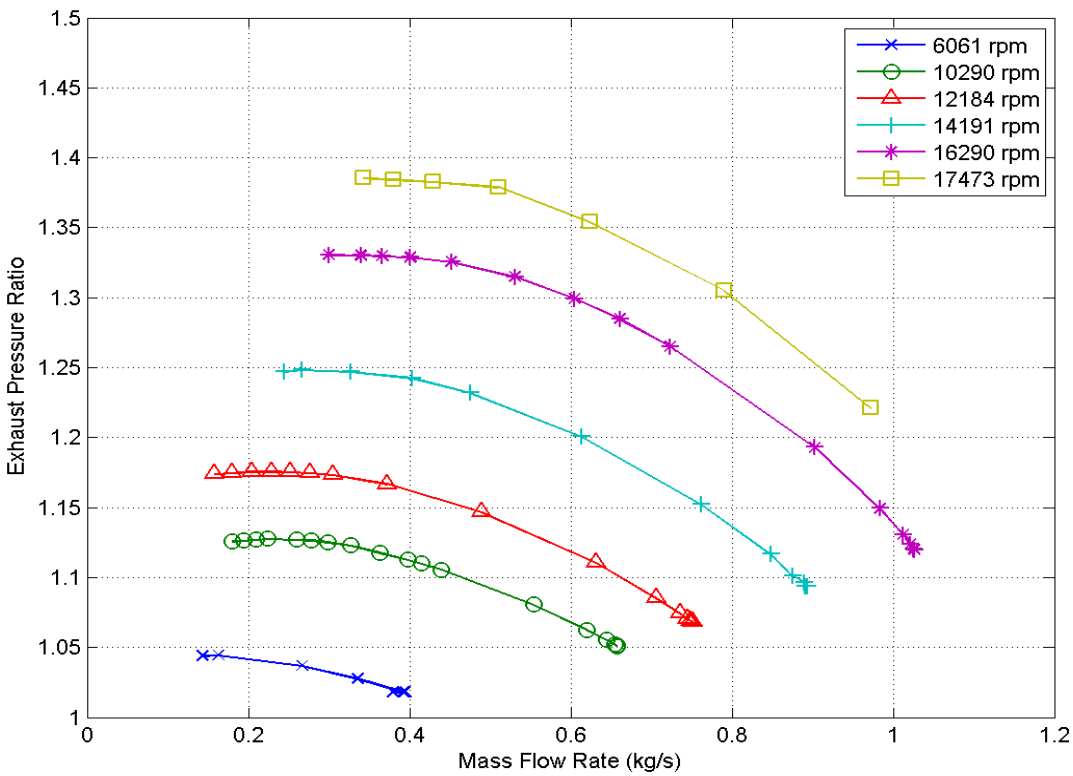

Figure 5.2 Compressor characteristic curves at different operating speeds.

The H_∞ design method is usually used with unstructured uncertainties, and it will provide good level of robustness for the system when designed properly. The interconnected system for

the synthesis of the surge controller is shown in Figure 5.3. The control input to the plant G(s) is the impeller tip clearance δ_{cl}, and the measured output for the controller is the linearized state corresponding to the plenum pressure rise and compressor mass flow rate.

According to the interconnected system in Figure 5.3, the input-output transfer function matrix is given as

$$\begin{bmatrix} z_1 \\ z_2 \end{bmatrix} = \begin{bmatrix} -W_1\, S_i\, K\, G\, W_3 & W_1\, S_i\, K\, W_4 \\ W_2\, S_o\, G\, W_3 & W_2\, S_o\, G\, K\, W_4 \end{bmatrix} \begin{bmatrix} w_1 \\ w_2 \end{bmatrix}, \tag{5.10}$$

where G is the transfer function of the compression system and K is the transfer function of the controller. W_i for i = 1 to 4 are the weighting functions for the H∞ controller and

$$S_i = (\mathrm{I} + K\, G)^{-1}, \tag{5.11a}$$

$$S_o = (\mathrm{I} + G\, K)^{-1}. \tag{5.11b}$$

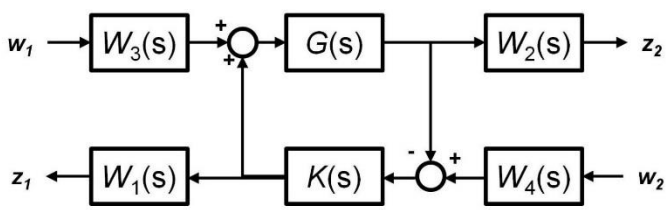

Figure 5.3 Interconnected system for the synthesis of the surge controller [1]

The main objective to be accomplished when designing the H_∞ controller is to minimize the H_∞ norm for the closed-loop system. The selection of the weighting functions is based on achieving this objective and the design requirements. In this case, W_1 and W_3 were chosen to satisfy the robustness condition of the interaction between the surge controller and the levitation controller. In addition, "W_4 was selected to prioritize the pressure feedback signal for the computation of the control input" [1]. The selected weighting functions for the H_∞ controller were

$$W_1 = I, \tag{5.12a}$$

$$W_2 = 0.001I, \tag{5.12b}$$

$$W_3 = \frac{2(s+0.1)}{s+300} I, \tag{5.12c}$$

$$W_4 = \frac{2000(s+0.1)}{s+3000} \begin{bmatrix} 1.5 & 0 \\ 0 & 1 \end{bmatrix}. \tag{5.12d}$$

This controller achieved the stability and robustness conditions for the design. In addition, it was observed that the bandwidth of the controller is within the limitation of the digital implementation.

5.3 Gain-Scheduled Controller Design

In this section, the gain-scheduled controller for compressor surge control is presented. As mentioned before, the throttle valve opening of 17% was selected to be the nominal opening, and the gain-scheduled controller was designed to stabilize the compression system beyond the nominal throttle valve opening. By decreasing the throttle opening, the flow will be restricted, and the system will start to become unstable. The previous controller design can stabilize the system for a throttle opening down to 17% and within a very small region around it. A gain-scheduled controller can potentially extend the stable operating region for the surge controller, while also achieving a high level of robustness.

Our goal is to extend the stable operating region of the compressor, which will allow it to operate deeper in the unstable operating region of the characteristic curve. Figure 5.4 illustrates a general shape of the compressor characteristic curve. The surge point is located approximately at the peak of the characteristic curve, and it separates the stable operating region on the right-hand side and the unstable region on the left-hand side. The surge curve is formed when connecting the surge points corresponding to different operating speeds. The authors in [1] used the throttle valve opening of 17% to linearize the compression system model, which will also serve as a starting

point of our gain-scheduled controller. By decreasing the valve opening, the flow will be restricted below the surge point. As a result, surge will occur. At the throttle opening of 11%, the system once again becomes stable, and this is expected. This can be justified due to changing of the slope of the characteristic curve.

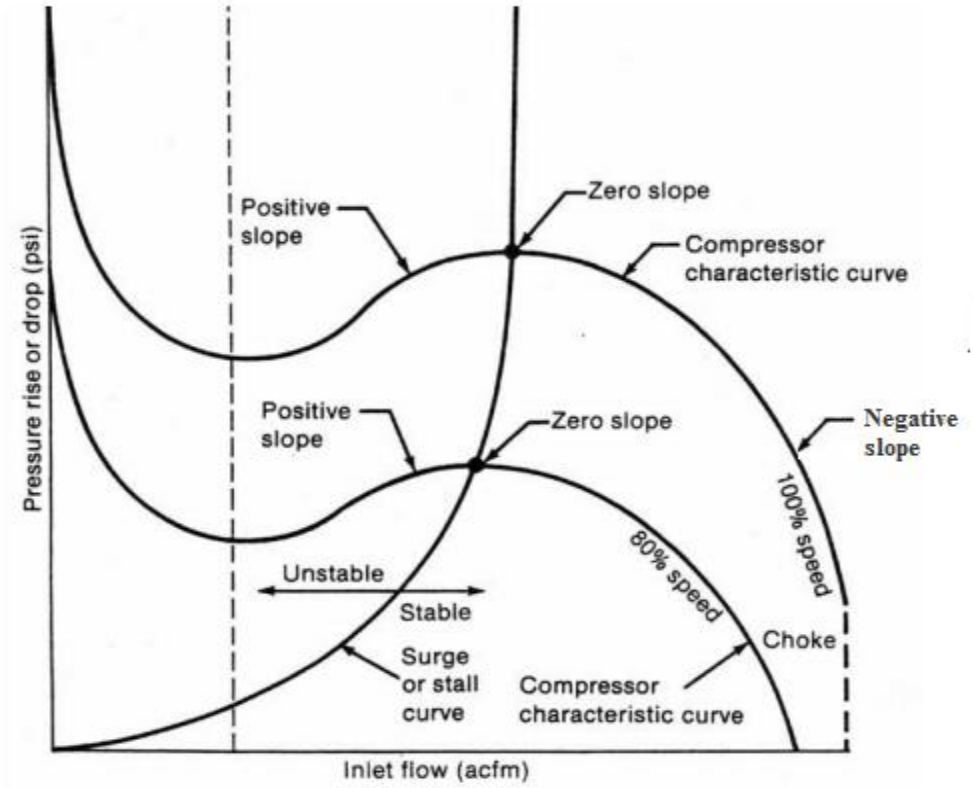

Figure 5.4 A general compressor characteristic curve [35]

In Figure 5.4, we can see the variation in the slope of the characteristic curve. The curve has a negative slope in the stable region. This slope becomes positive when the compressor starts to operate in the unstable region. If the flow is further restricted, the slope becomes negative, which corresponds to a stable equilibrium flow region. This clarifies the behavior of the system at the opening 11%. Figure 5.5 shows the numerical simulation of the plenum pressure rise 11% throttle valve opening.

For the gain-scheduled controller design, the throttle valve opening was set to be between 12% and 17%, with operating sections divided by a step size of 1%. This results in six throttle valve openings, and six linear controllers are designed for these opening values. The throttle valve opening was chosen to be the scheduling variable, which determines the switching between the controllers. Figure 5.6 shows the operating range of the gain scheduling controller with respect to the scheduling signal.

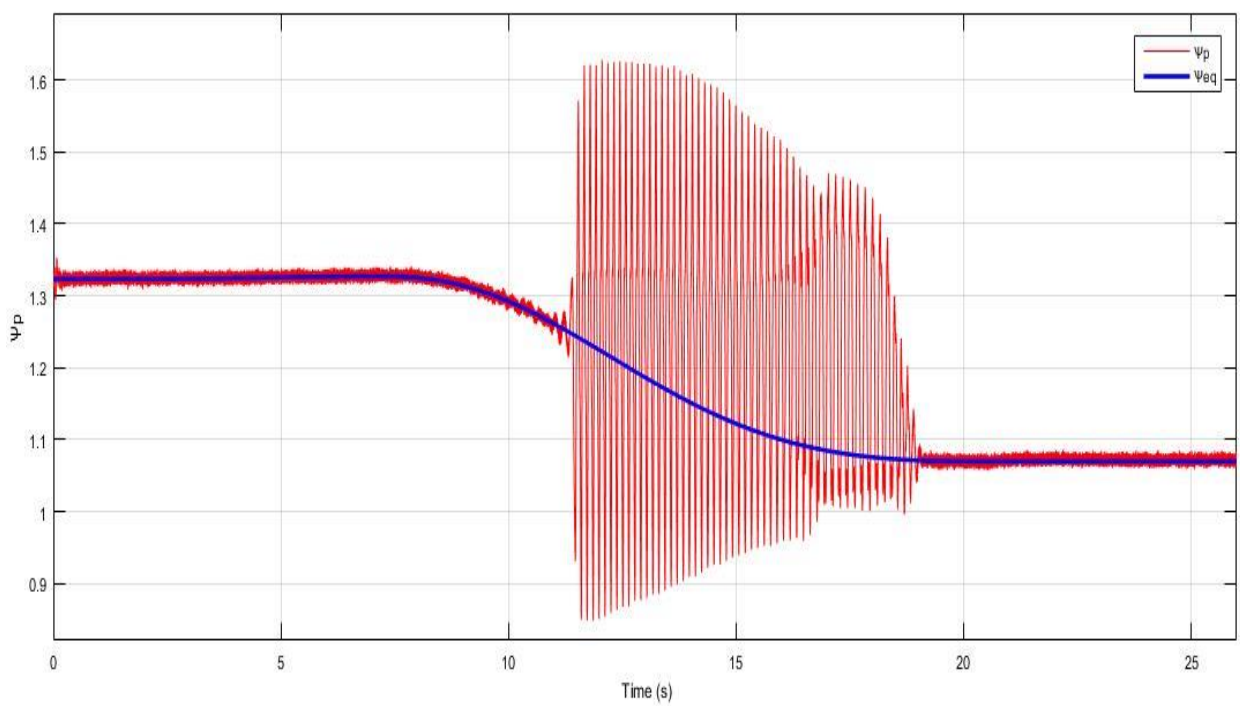

Figure 5.5 Plenum pressure rise for throttle valve opening of 11%

The behavior of the gain-scheduled controller is as follows. When the throttle opening is 17% or more, the gain-scheduled controller will turn controller 1 on to stabilize the compressor surge. As the throttle opening is decreased to 16%, the scheduled controller will switch to controller 2, which will stabilize the system for all the openings between 16% and 17%. In the same manner, controller 3 will stabilize the compression system for all the opening between 15% and 16%, and controller 4 for all the opening between 14% and 15%, and so on. A delay is

introduced in the switching between the controllers to mitigate the effect of noise in the switching signal. The observer-based technique was used to achieve bumpless and smooth transfer when switching between the controllers.

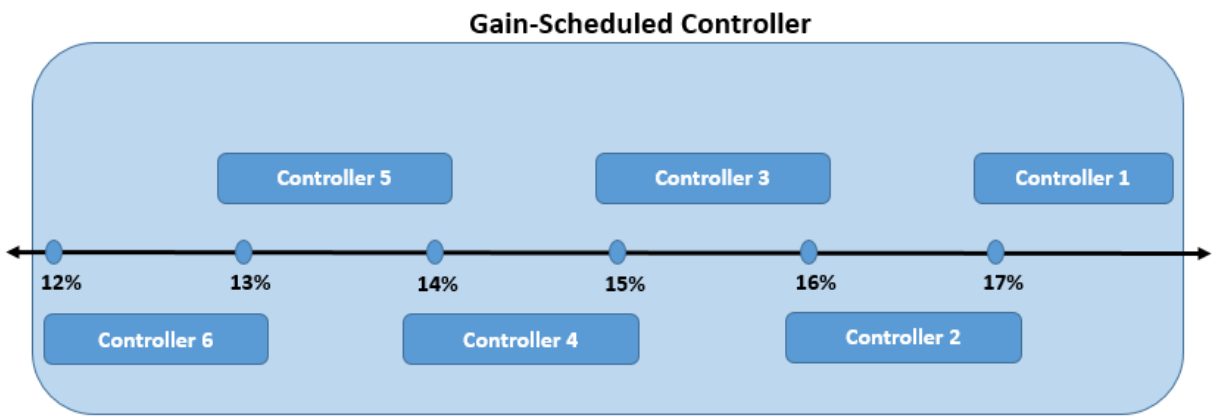

Figure 5.6 Resulting gain-scheduled controller

The design of the linear H_∞ controller requires the selection of the weighting functions to achieve stability, performance, and robustness requirements. There are several techniques to select the weighting functions [10]. The majority of these techniques use a trial and error selection process to find the appropriate weighting functions. In some cases, the designer may not be able to find the weighting functions that will result in the stabilizing controller, and this is the main disadvantage of the trial and error method. In our design, the weighting functions of the controllers are tuned from the design in [1] within certain limits using the trial and error method. The objective is to achieves similar robustness and stability conditions at the different linearization points.

In the linear controller design, we found that W_3 and W_4 have the most effect on the controller performance by the trial and error method. The weighting functions of the five linear controllers in the gain-scheduled controller were selected to achieve the performance objectives describes in Section 5.2. The weighting functions for the controllers 2 through 6 were found to be

- **<u>Controller 2</u>**

$W_1 = I,$ (5.14a)

$W_2 = 0.001\, I,$ (5.14b)

$W_3 = \frac{2(s+0.3)}{s+400}\, I,$ (5.14c)

$W_4 = \frac{1500(s+0.6)}{s+2700}\, I.$ (5.14d)

- **<u>Controller 3</u>**

$W_1 = I,$ (5.15a)

$W_2 = 0.001\, I,$ (5.15b)

$W_3 = \frac{2(s+2.5)}{s+500}\, I,$ (5.15c)

$W_4 = \frac{1700(s+0.5)}{s+1600}\, I.$ (5.15d)

- **<u>Controller 4</u>**

$W_1 = I,$ (5.16a)

$W_2 = 0.001\, I,$ (5.16b)

$W_3 = \frac{s+0.7}{s+800}\, I,$ (5.16c)

$W_4 = \frac{1300(s+0.3)}{s+2000}\, I.$ (5.16d)

- **<u>Controller 5</u>**

$W_1 = I,$ (5.17a)

$W_2 = 0.001\, I,$ (5.17b)

$$W_3 = \frac{2.5(s+0.5)}{s+600} I, \tag{5.17c}$$

$$W_4 = \frac{1900(s+0.9)}{s+1700} I. \tag{5.17d}$$

- **<u>Controller 6</u>**

$$W_1 = I, \tag{5.18a}$$

$$W_2 = 0.001\, I, \tag{5.18b}$$

$$W_3 = \frac{1.3(s+0.8)}{s+700} I, \tag{5.18c}$$

$$W_4 = \frac{2300(s+0.4)}{s+2100} I. \tag{5.18d}$$

Figure 5.7 shows the magnitude of the interconnected system in Figure 5.3 with the weighting functions and linear controller corresponding to the throttle valve opening at 12%. Similar results were obtained for the linear controllers designed for the remaining throttle valve opening values.

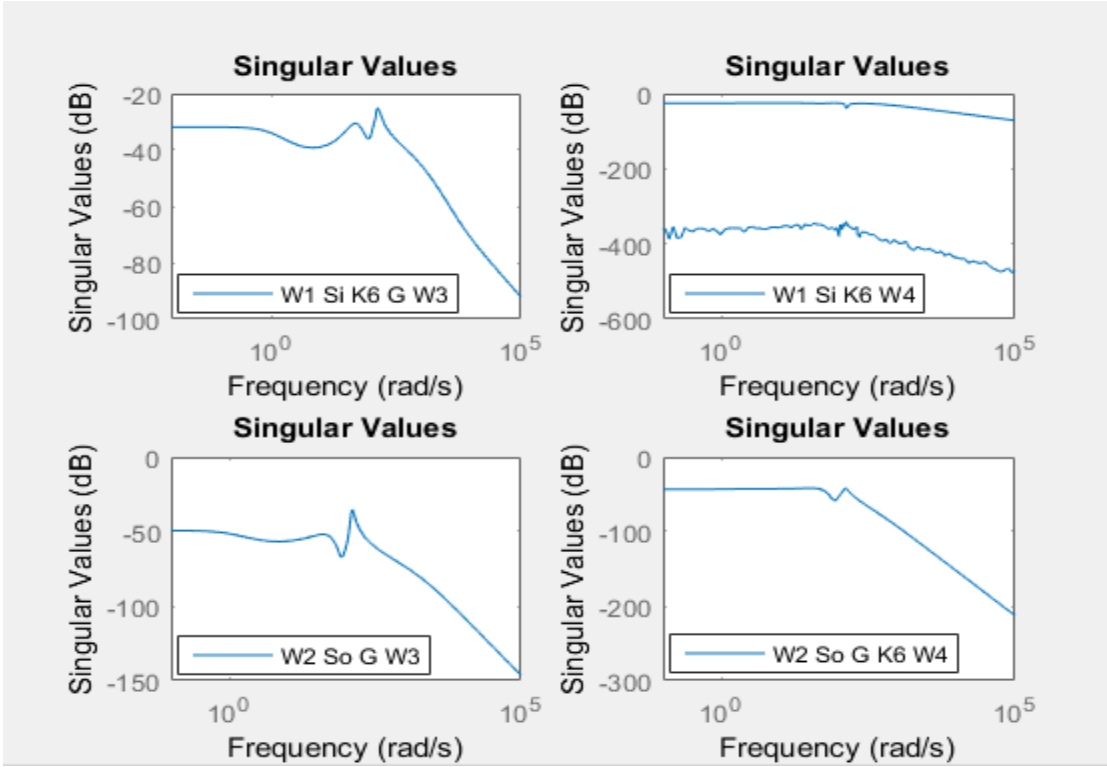

Figure 5.7 Magnitude of the interconnected system for throttle opening of 12%

5.4 Simulation Results

In order to verify the performance of the gain-scheduled surge controller, a simulation test was constructed using Simulink. The compression system was represented using the nonlinear surge model in Equation (5.9). The control signal is the impeller tip clearance δ_{cl}. A saturation block and a low pass filter were added to the control signal to represent the physical limitations of the actuator. In addition, we added Gaussian noise to the feedback pressure signal with a mean of 0 and variance of $1\text{x}10^{-5}$.

To demonstrate the performance of our gain-scheduled controller, we compared it to the single H_∞ surge controller from [1]. Figures 5.8 through 5.11 shows the simulated response of the compression system with the surge controller in [1]. In this numerical example, we gradually

changed the throttle valve opening from 20% to 12% in 25 seconds. This drove the compression system to surge condition.

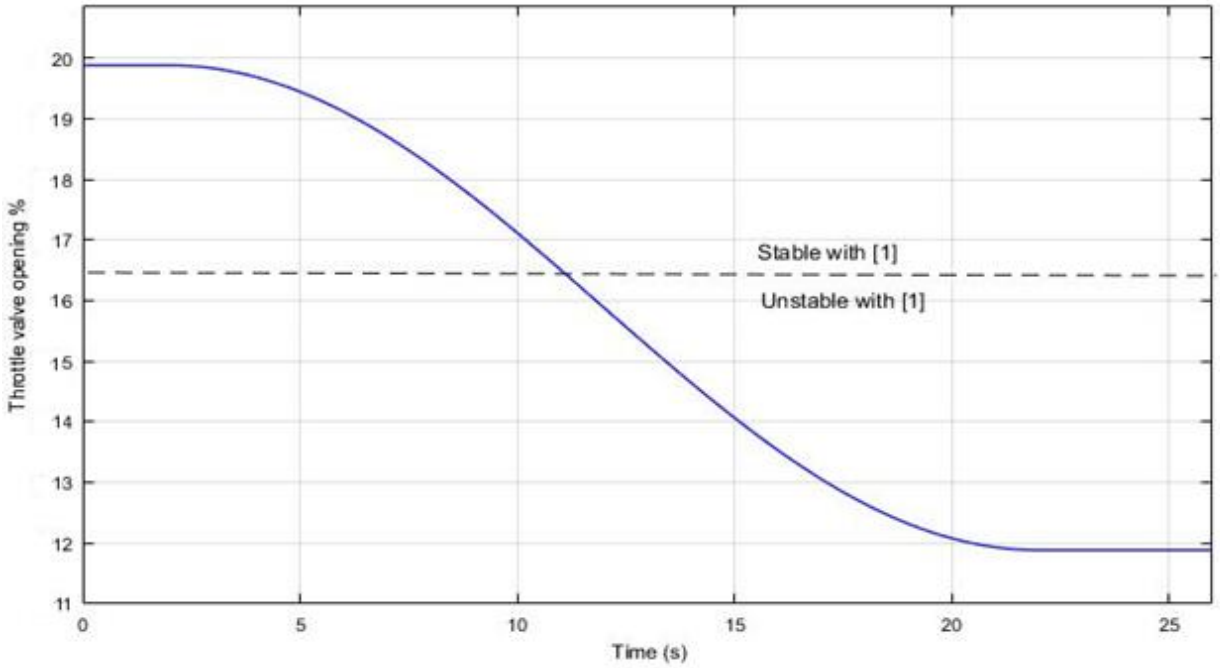

Figure 5.8 Throttle valve opening

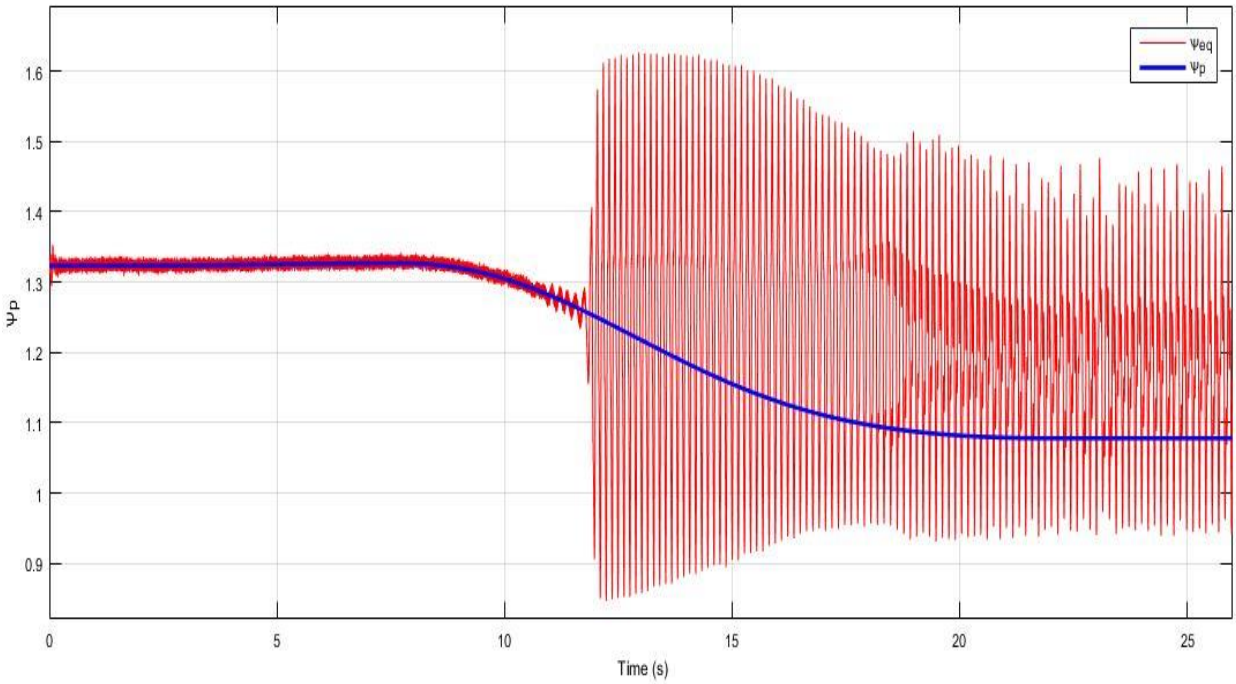

Figure 5.9 Plenum pressure rise

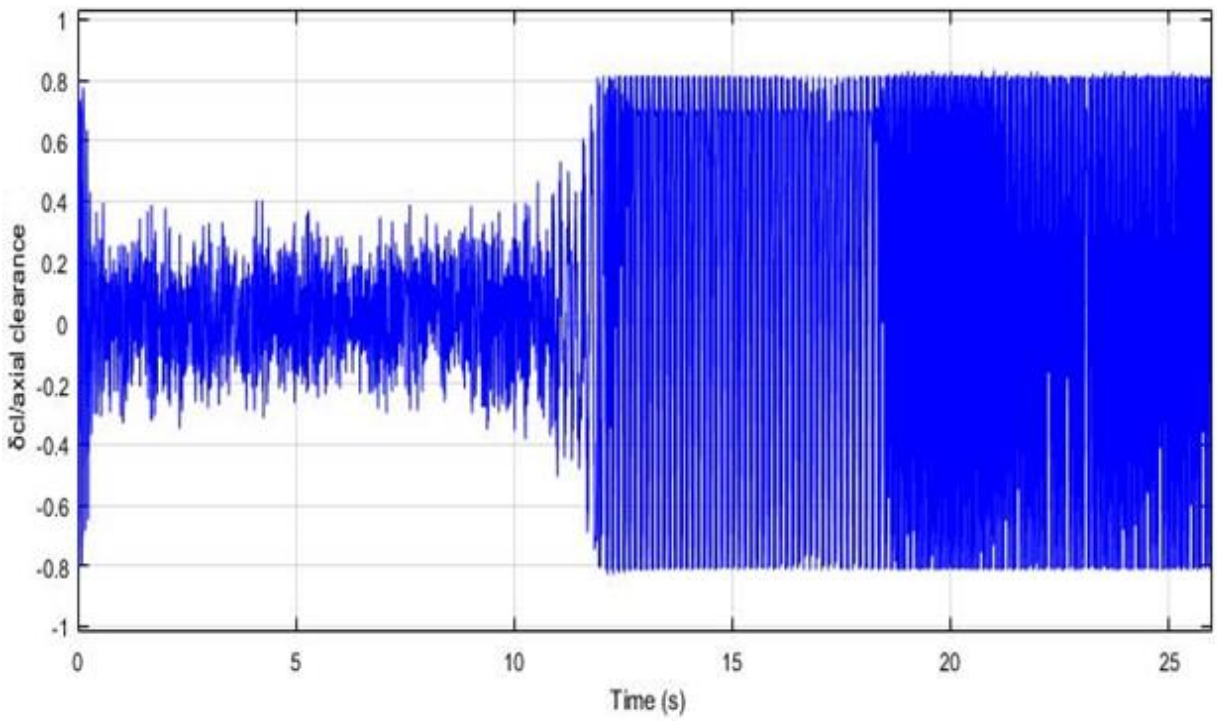

Figure 5.10 δ_{cl}(t) with the single surge controller in [1]

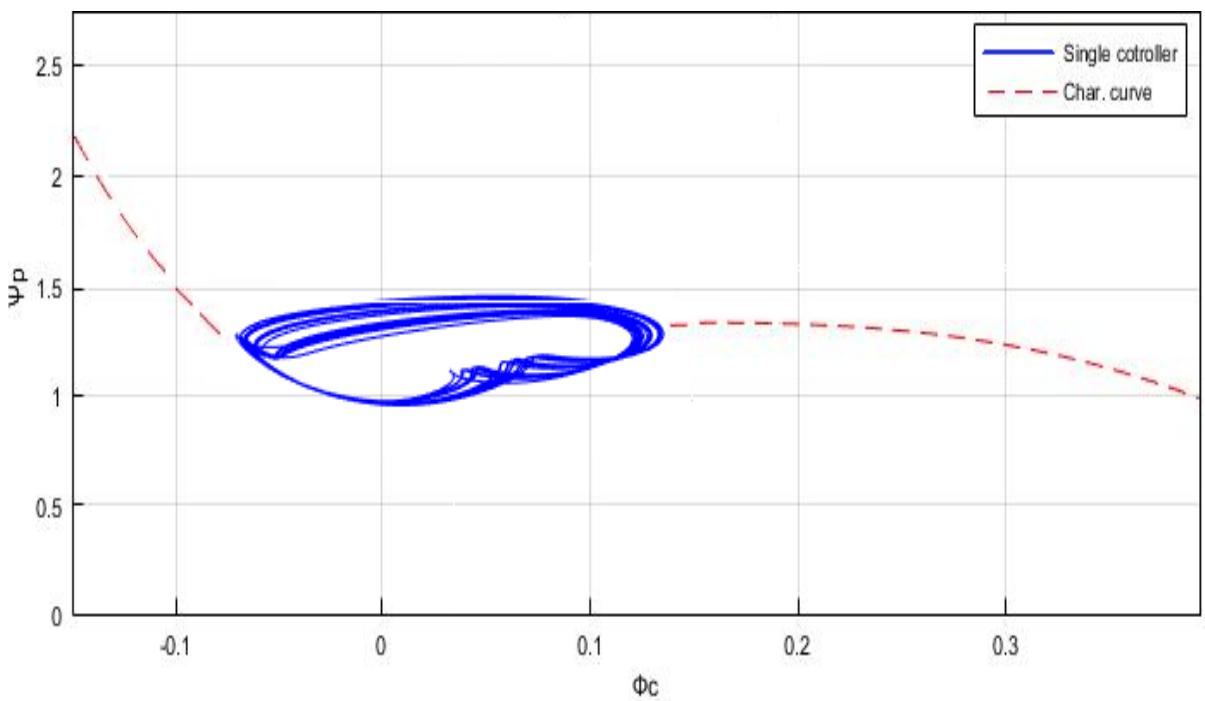

Figure 5.11 Operation of the system using the controller in [1]

Figure 5.8 shows the throttle valve opening signal. It also marks the limit in the throttle valve opening at which the system under the controller from [1] becomes unstable. Figure 5.8 illustrates the throttle valve opening and how the system's stability changes when changing the valve opening. Figure 5.9 shows the simulated plenum pressure rise signal together with the equilibrium pressure rise from the characteristic curve. It is obvious from the figure that the system becomes unstable and the controller we are using is not regulating the flow. The control signal of the simulation case is shown in Figure 5.10. We can see how the system becomes unstable when the throttle valve opening is around 16%. In addition, a clipping in the control signal occurred because the controller exceeded the saturation limits. Figure 5.11 presents the plenum pressure rise as function of the compressor mass flow rate together with the compressor characteristic curve. We can see that the compressor falls in the surge limit cycle, which demonstrates that the system is unstable.

From these figures, we can see that the controller in [1] was not able to stabilize the system under the new conditions. Figures 5.12 through 5.14 illustrates the simulated response of the system when using the gain-scheduled controller. In Figure 5.12, it is obvious how the plenum pressure rise matches the equilibrium pressure rise. The gain-scheduled surge controller stabilizes the compression system with the control signal shown in Figure 5.13. It is obvious how the controller worked to stabilize the system without entering the saturation mode. Figure 5.14 shows the behavior of the system and how it is running without any surge limit cycles using the gain-scheduled controller. The gain-scheduled controller was able to stabilize the compression system when entering the unstable region between the compressor mass flow rates of 1.2 and -0.015,

which indicates that it extended the stable operating region down to the valve opening of 12% instead of 17%.

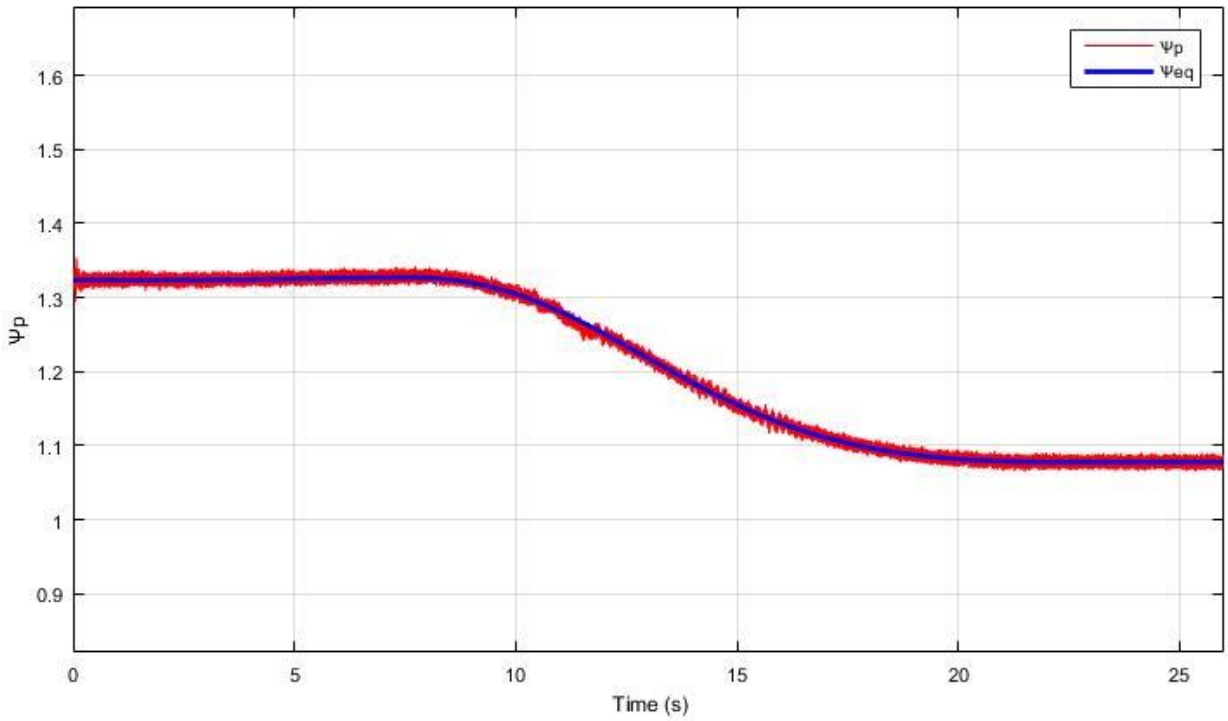

Figure 5.12 Plenum pressure rise with the gain-scheduled controller

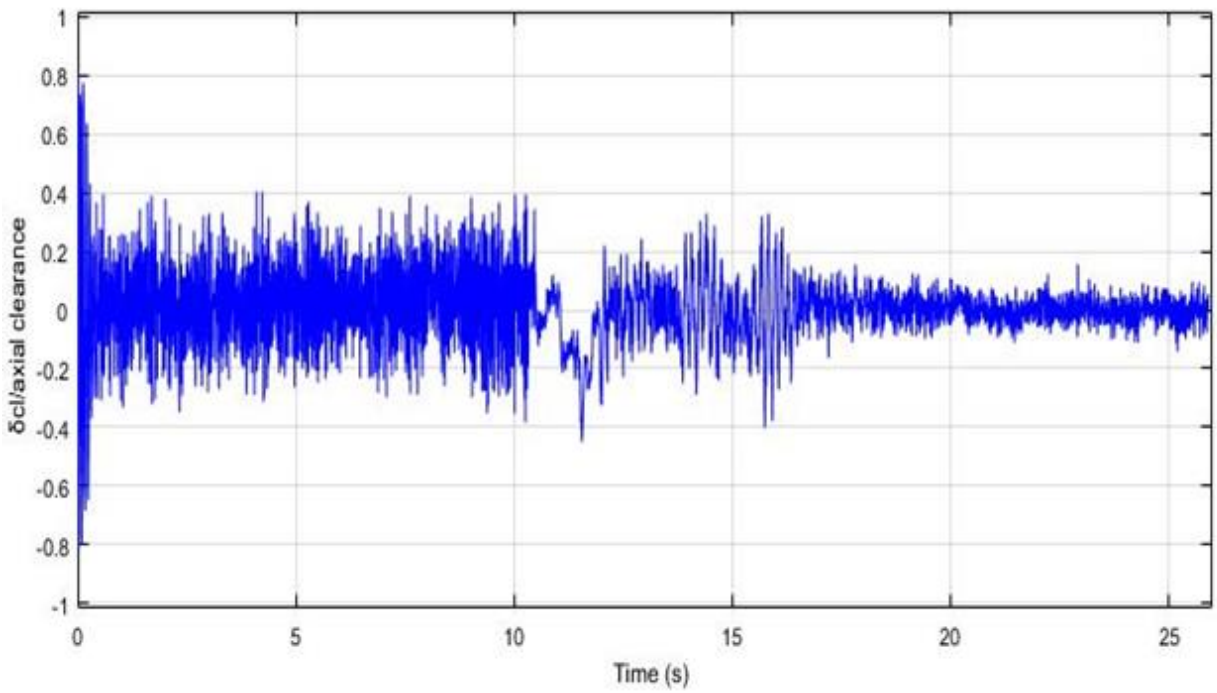

Figure 5.13 δ_{cl}(t) with the gain-scheduled surge controller

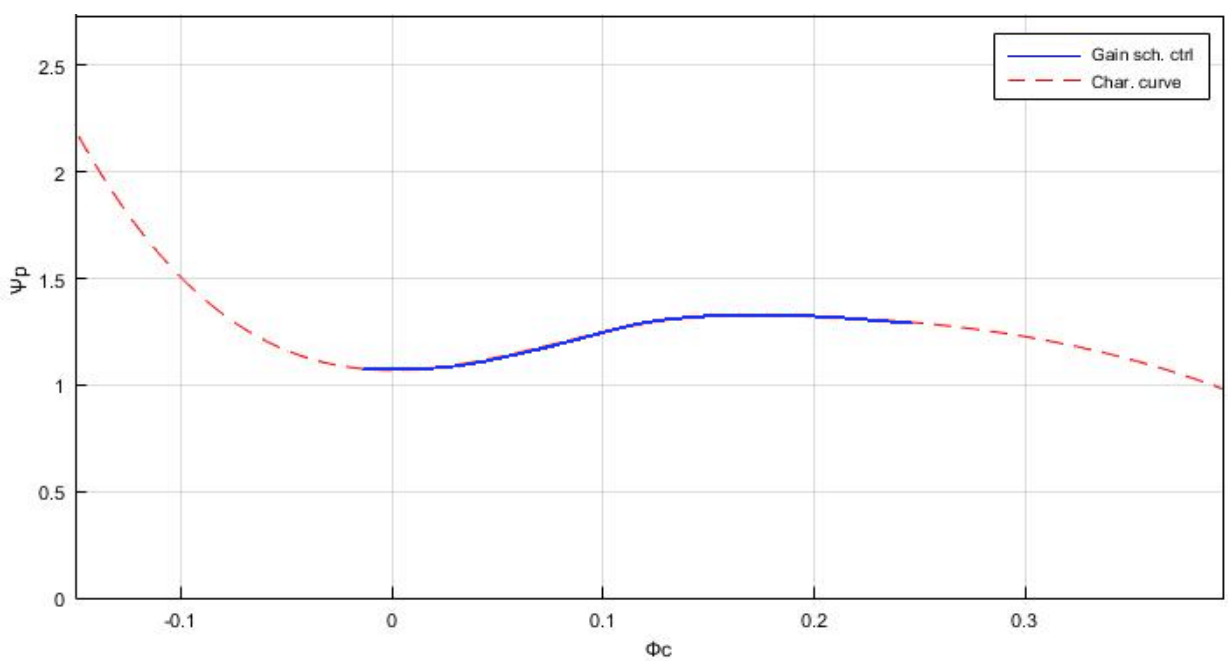

Figure 5.14 Operation of the system using the gain-scheduled controller

5.5 Conclusion

In this chapter, we presented the design of the compression system and surge controller designs that were introduced in [1]. In addition, we presented the design of the gain-scheduled controller. This controller was designed to extend the stable operation region of the compression system. It allows the compression system to operate with a throttle valve opening as low as 12%. A Gaussian noise was added in the simulation design and the controller design accommodated the noise. This means that the compression system has a higher level of robustness against the disturbances with this controller compared to the previous controller [1]. The gain-scheduled controller consists of six linear controllers. A smooth transfer between the controllers was achieved using the observer-based technique.

Chapter 6

Conclusions and Future Work

The use of the gain-scheduled controller to stabilize compressor surge and control the AMB levitation was discussed in this thesis. The motivations and objectives of this work were introduced in Chapter 1. In Chapter 2, we presented a brief introduction to compressors and some of the common instabilities in compressors. Active magnetic bearings were also introduced here.

In Chapter 3, linear control systems were introduced. Advanced control methods were discussed in this chapter such as the H_∞ control and the μ-synthesis control techniques. In addition, we presented the concept of the gain scheduling control method and its main classifications, along with its advantages and disadvantages. In Chapter 4, we presented a case study of a gain scheduled controller designed for the stabilization of a rotor-AMB system. In order to guarantee the performance over a wide operating speed range, the μ-synthesis control method was used to design the linear controllers that forms the gain-scheduled controller.

Chapter 5 presented the compression system model and the design of the single H_∞ surge controller in [1]. As a continuation to this work, we designed a gain-scheduled controller to extend the stable operating region of the compression system and improve the robustness of the closed-loop system. The scheduling signal for the controller was chosen to be the throttle valve opening. The gain-scheduled controller was tested through a numerical simulation, and compared to the results with the controller in [1]. We were able to demonstrate that the gain-scheduled controller

can stabilize the system down to a throttle valve opening of 12%. Simulation results also showed the smooth transfer when switching between the controllers.

The compressor characteristic curve presented the gas pressure rise as a function of the mass flow rate. The linear controllers were designed based on known equilibrium points for the system at each throttle valve opening at the rotating speed of 16290 rpm, where the equilibrium point is the intersection between the characteristic curve and the load curve. Figure 5.2 shows the compressor characteristic curve for different operating speeds with both stable and unstable regions. The curve in the unstable operating region is estimated from the curve in the stable operating region using the 3rd order polynomial interpolation. This adds uncertainties for the feedback control and limits the performance of the controllers. This problem can be solved if the controllers are designed based on unknown equilibrium points. There are several techniques that can be used with the unknown steady states such as adaptive control and delayed-feedback control. As a future work, these techniques and others will be tested for the system and the see the effectiveness of the controllers.

References

[1] Yoon, Se Young, Zongli Lin, and Paul E. Allaire. *Control of Surge in Centrifugal Compressors by Active Magnetic Bearings: Theory and Implementation*. Springer Science & Business Media, 2012.

[2] Boyce, Meherwan P. *Centrifugal compressors: a basic guide*. PennWell Books, 2003.

[3] Bloch, Heinz P. *A practical guide to compressor technology*. John Wiley & Sons, 2006.

[4] Ng, Eddie YK, and Ningyu Y. Liu. *Compressor instability with integral methods*. Springer Science & Business Media, 2007.

[5] Brennen, Christopher E. *Hydrodynamics of pumps*. Cambridge University Press, 2011.

[6] White, Robert C., and Rainer Kurz. "Surge avoidance for compressor systems." *Proceedings of the 35th Turbomachinery Symposium, George R. Brown Convention Center, Houston, Texas*. 2006.

[7] Ogata, Katsuhiko, and Yanjuan Yang. "Modern control engineering." (1970): 1.

[8] Nise, Norman S. *CONTROL SYSTEMS ENGINEERING, (With CD)*. John Wiley & Sons, 2007.

[9] Locatelli, Arturo. *Optimal control: An introduction*. Springer Science & Business Media, 2001.

[10] Bansal, Ankit, and Veena Sharma. "Design and Analysis of Robust H-infinity Controller." *Control Theory and Informatics* 3.2 (2013): 7-14.

[11] Hynynen, Katja, and Alexander Smirnov. "Case study comparison of linear H∞ loop-shaping design and signal-based H∞ control." *Information, Communication and Automation Technologies, 2009. ICAT 2009. XXII International Symposium on*. IEEE, 2009.

[12] Balas G., Packard A.. “The structure singular value (μ) framework” in the Control Handbook, pp 671-687. CRC Press, Boca Raton (1996).

[13] Shamma, Jeff S. "Analysis and design of gain scheduled control systems." PhD diss., Massachusetts Institute of Technology, 1988.

[14] Rugh, Wilson J., and Jeff S. Shamma. "Research on gain scheduling."*Automatica* 36.10 (2000): 1401-1425.

[15] Hanus, R., Kinnaert, M. and Henrotte, J.-L. (1987). “Conditioning technique, a general anti-windup and bumpless transfer method,” Automatica, Vol. 23, No. 6, pp. 729-739.

[16] ˚Astr¨om, K. and Wittenmark, B. (1997). Computer-Controlled Systems, Prentice-Hall, Upper Saddle River, NJ 07458.

[17] Li, G. Robust Stabilization of Rotor-Active Magnetic Bearing Systems. Thesis. Department of Mechanical and Aerospace Engineering Department of Electrical Engineering / University of Virginia, 2007.

[18] Naus, Ir. G. Gain Scheduling Robust Design and Automated Tuning of Automotive Controllers. Thesis. University of Technology Eindhoven (TU/e)/ Department of Mechanical Engineering, 2009. N.p.: n.p., n.d. Print.

[19] Chen, Jin-jun, and Zhi-cheng Ji. "The gain scheduling control for wind energy conversion system based on LPV model." *Networking, Sensing and Control (ICNSC), 2010 International Conference on*. IEEE, 2010.

[20] Rodriguez-Martinez, Arnulfo, and Raul Garduno-Ramirez. "PI fuzzy gain-scheduling speed con-trol of a gas turbine power plant." *Intelligent Systems Application to Power Systems, 2005. Proceedings of the 13th International Conference on*. IEEE, 2005.

[21] Ruzhekov, G., Ts Slavov, and T. Puleva. "Modeling and implementation of hydro turbine power adaptive control based on gain scheduling technique."*Intelligent System Application to Power Systems (ISAP), 2011 16th International Conference on*. IEEE, 2011.

[22] Ghosh, Falguni, and Indraneel Sen. "Design and Performance of a Local Gain Scheduling Power System Stabilizer for Inter-Connected System." (1991): Vol-1.

[23] Mohammadi-Milasi, R., M. J. Yazdanpanah, and P. Jabehdar-Maralani. "A novel adaptive gain-scheduling controller for synchronous generator." *Control Applications, 2004. Proceedings of the 2004 IEEE International Conference on*. Vol. 1. IEEE, 2004.

[24] Schweitzer, G., E. Maslen, H. Bleuler, M. Cole, P. Keogh, R. Larsonneur, R. Nordmann, and A. Traxler. Magnetic Bearings: Theory, Design, and Application to Rotating Machinery. Dordrecht: Springer, 2009. Print.

[25] Knospe, Carl, and Charles Yang. "*Gain-Scheduled Control of a Magnetic Bearing with Low Bias Flux*." *Decision and Control, 1997., Proceedings of the 36th IEEE Conference on*. Vol. 1. IEEE, 1997.

[26] Mohamed, Abdelfatah M., Ikbal MM Hassan, and Adel MK Hashem. "Elimination of imbalance vibrations in magnetic bearing systems using discrete-time gain-scheduled Q-parametrization controllers." *Control Applications, 1999. Proceedings of the 1999 IEEE International Conference on*. Vol. 1. IEEE, 1999.

[27] Veselý, Vojtech, and Adrian Ilka. "Gain-scheduled PID controller design."*Journal of process control* 23.8 (2013): 1141-1148.

[28] Greitzer, Edward M. "Surge and rotating stall in axial flow compressors—Part I: Theoretical compression system model." *Journal of Engineering for Power* 98.2 (1976): 190-198.

[29] Goodson, R. E., and R. G. Leonard. "A survey of modeling techniques for fluid line transients." *Journal of Basic Engineering* 94.2 (1972): 474-482.

[30] Krus, Petter, Kenneth Weddfelt, and Jan-Ove Palmberg. "Fast pipeline models for simulation of hydraulic systems." *Journal of dynamic systems, measurement, and control* 116.1 (1994): 132-136.

[31] McMillan, Gregory K. *Centrifugal and Axial Compressor Control*. Momentum Press, 2010.

[32] Moore, Franklin K., and Edward Marc Greitzer. "A theory of post-stall transients in axial compression systems: Part I—Development of equations." *Journal of engineering for gas turbines and power* 108.1 (1986): 68-76.

[33] Matsumura, Fumio, et al. "Application of gain scheduled H∞ robust controllers to a magnetic bearing." *IEEE Transactions on Control Systems Technology* 4.5 (1996): 484-493.